OPEN-SYSTEM DEGASSING OF A FRACTIONATING, ALKALINE MAGMA, MOUNT EREBUS, ROSS ISLAND, ANTARCTICA

ALAN JOSEPH ESCHENBACHER

Submitted in Partial Fulfillment
of the requirements for the Degree of
Masters of Science in Geochemistry

New Mexico Institute of Mining and Technology

Socorro, New Mexico

December, 1998

TABLE OF CONTENTS

LIST OF TABLES

LIST OF FIGURES

ABSTRACT

Mount Erebus is an active, intraplate, alkaline volcano located on of Ross Island, Antarctica. The volcano is composed predominantly of phonolite lavas with lesser amounts of basanite, phonotephrite and tephriphonolite. These lava compositions define a nearly continuous differentiation lineage. The main crater contains an actively convecting, anorthoclase phonolite lava lake that produces frequent strombolian eruptions and a continuous gas plume.

The composition of melt inclusions (MI) from the compositional range of lavas, determined by electron microprobe and ion probe closely follow the trend of the bulk rock composition and mimic fractional crystallization models (Kyle et al., 1992). The incompatible trace elements (Li, B, Rb, Zr, Th) exhibit a factor of four increase in concentration through the compositional range of melt inclusions that is consistent with phonolite being a 25% residual liquid produced from a basanite parent melt.

Water concentrations in basanite MI range from 1.15 to 1.75 wt%. With the exception of a tephriphonolite sample (97009) with an average 0.5% wt% H_2O, all other samples have H_2O contents near 0.1 wt%. Carbon dioxide contents of basanite MI range from 4000-7300 ppm. Most other samples have CO_2 contents less than 2000 ppm. Sample 97009 ranges from 1500 to 3600 ppm CO_2. Sulfur contents of melt inclusions exhibit a decreasing trend from basanite (~2500 ppm) to phonolite (~400 ppm). The sulfur content correlates closely with Fe content. Basanite MI are enriched in S above the Fe-S trend suggesting sulfur solubility is enhanced in the basanite. Fluorine concentrations in MI remain somewhat constant through the range of melt compositions.

Average fluorine contents range from ~1600 to 2600 ppm. Chlorine concentrations of MI show an increasing trend from 740 ppm in basanite to 1500 ppm in phonolite.

The degassing of CO_2, H_2O, and S is nearly complete as the concentration of the volatiles decrease dramatically through the compositional range of lavas. The small fraction of F and Cl lost is probably due to distillation of these elements by the H_2O-bearing fluid phase.

The H_2O and CO_2 contents of MI in the tephrite and phonolite compositions suggest depth of crystallization and therefore depth of the magma chambers. The calculated saturation pressures of ~1 kbar indicate crystal growth occurred in magma chambers that resided at shallow depths (<5 km).

The CO_2 and H_2O contents of the basanite MI indicate vapor saturation pressures of 3-4.5 kbar and minimum inclusion trapping depth of 8-13 km. The basanite magma these MI represent must degas a CO_2-rich fluid (~90 mole% CO_2) at these pressures.

Theoretical gas fluxes produced by open system degassing of a magma system differentiating from basanite to phonolite closely resemble the observed gas fluxes for SO_2, HF, and HCl from the Mount Erebus lava lake. The theoretical CO_2 flux of the system is much less than the observed flux. The large CO_2 flux observed emanating from the volcano must be derived from magma deeper in the system than the melt inclusions are recording (~13 km), possibly as deep as the mantle. The evidence of open system degassing of a CO_2-rich fluid from great depths is consistent with experimental studies that suggest a carbonated mantle source is necessary to produce alkaline, silica-undersaturated magmas such as basanite.

ACKNOWLEDGEMENTS

This work would not have been possible without the field knowledge and assistance of Drs. Philip Kyle and Kurt Panter. Special thanks go to Diane Winter and Dr. David Harwood for locating and donating the Dry Valley Drilling Project drill core samples. I would like to thank Dr. Jacob Lowenstern of the U.S. Geological Survey for allowing me to use the FTIR facilities at the U.S.G.S., and for offering his extensive knowledge of the technique and implications of the results. I wish to thank Dr. Nelia Dunbar for use of the electron microprobe at New Mexico Tech, and for her careful instruction on how to use the instrument. I thank Dr. Richard Hervig of Arizona State University for his constant support in operating the ion probe at ASU. This work has benefited greatly from discussions with Drs. Philip Kyle, Nelia Dunbar, Andrew Campbell, Jacob Lowenstern, and Tom Sisson.

Support for this research came from National Science Foundation grant OPP-9419267 to Philip Kyle.

INTRODUCTION

Dissolved volatile contents of melt inclusions (MI) trapped in phenocrysts can be used to determine the pre-eruptive volatile content of magma (Johnson et al., 1994; Lowenstern, 1995). Melt inclusions are representative of the undegassed magma provided that the inclusions remained sealed during eruption and deposition, and did not undergo post-entrapment crystallization. Well-preserved melt inclusions provide valuable information about processes such as fractional crystallization and degassing of magmatic systems.

Many studies have used pre-eruptive volatile contents of melt inclusions to estimate the amount of various gases evolved during volcanic activity. The petrologic estimate of degassing is often a small fraction of the measured gas flux from an active volcano (Andres et al., 1991; Westrich and Gerlach, 1992; Gerlach and McGee, 1994; Allard et al., 1994; Kazahaya, et al., 1994; Allard, 1997). The petrologic estimate of degassing uses the comparison of volatile contents of melt inclusions and matrix glasses in conjunction with amount of magma erupted to estimate the amount of volatiles released during eruption. Mount Erebus, Antarctica also exhibits a large disparity between the observed gas emissions from the vent and the amount of gas that can be attributed to degassing of erupted magma (Kyle et al., 1982; Kyle et al., 1990). Other sources of volatiles that are commonly called upon are degassing of magma deeper in the system and existence of a separate fluid phase coexisting with the magma.

In this study, the pre-eruptive volatile contents in melt inclusions were measured on the recently erupted anorthoclase phonolite bombs and a series of older, more primitive rock compositions. The melt inclusions record a sequence of melt compositions

from basanite to phonolite that are related through fractional crystallization. The objective of this study is to use the pre-eruptive volatile content of this fractional crystallization sequence to ascertain the probable source of excess volatiles in the Mount Erebus magmatic system.

GEOLOGIC BACKGROUND

Mount Erebus is an active, intraplate, alkaline volcano located in the central portion of Ross Island (Figure 1). The volcano is surrounded by three adjacent vent areas, Mount Bird, Mount Terror, and Hut Point Peninsula. Mount Erebus contains a persistent, convecting, anorthoclase phonolite lava lake. Small Strombolian eruptions occur daily in the lava lake. This activity has been continuous since the first scientific observations in 1972 and probably since the volcano's discovery in 1841 (Kyle et al., 1982). Despite the continuous nature of the activity, very little material is erupted out of the crater. Few bombs are thrown clear of the lava lake, therefore much of the lava is recycled by convection.

The gas plume related to the lava lake activity has been the subject of recent studies. Recent (post 1984 activity) emission rates of volatiles are as follows: HF = 6-25 Mg/day, HCl = 15-48 Mg/day, SO_2 = 21-71 Mg/day (Kyle et al., 1990; Zreda-Gostynska et al., 1997), and CO_2 ~ 2000 Mg/day (L.J. Wardell, pers. comm.). These fluxes, especially CO_2, suggest sources other than the erupted phonolite lava contribute to the gas plume.

Mount Erebus is composed predominantly of anorthoclase phonolite lavas. However, basanite, phonotephrite, and tephriphonolite lavas crop out in eroded volcanic cones that form islands and sea cliffs on the southwest side of Mount Erebus and Hut

Point Peninsula (Moore and Kyle, 1987). These lava compositions form a fractional crystallization sequence from basanite to phonolite (Kyle et al., 1992).

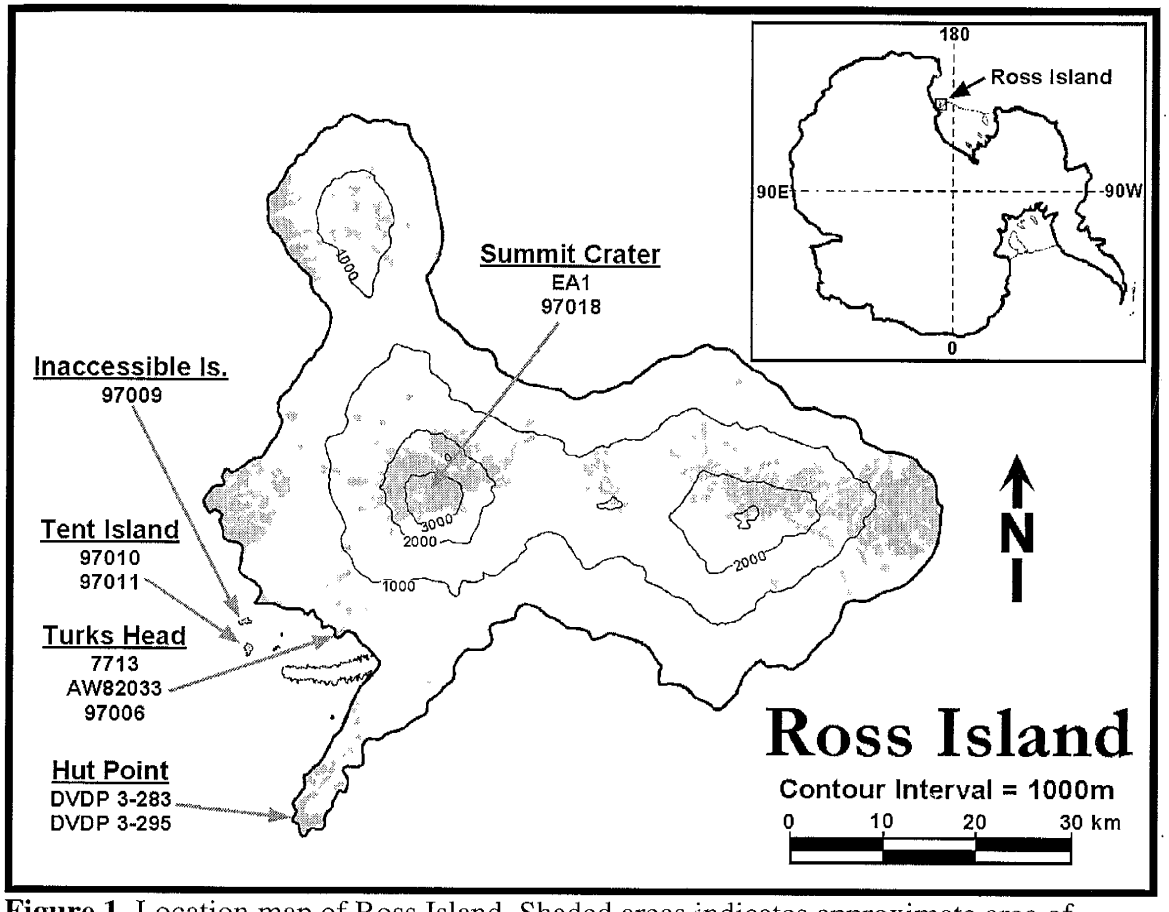

Figure 1. Location map of Ross Island. Shaded areas indicates approximate area of outcrop. Samples listed under geographic location.

METHODS

Samples

Samples were collected from Hut Point Peninsula (basanite), Inaccessible and Tent Islands (tephriphonolite), Turks Head (basanite, phonotephrite, tephriphonolite) and from the summit of Mount Erebus (phonolite)(Figure 1; Appendix A). Samples DVDP 3-283, 3-295, AW82033, 7713, 97009, 97010, and 97011 are hyaloclastites. Sample 97006 is a highly vesicular lava flow top. Sample 97018 is a fresh bomb erupted in 1997 and EA1 is a crystal from a bomb. These samples were selected because they cooled very

quickly upon eruption. Rapid cooling quenches the melt inclusions to a glass, thus preserving the melt from post entrapment crystallization. Only glassy inclusions without evidence of leaking or cracking were selected for study.

Fourier Transform Infrared Spectroscopy

The concentrations of dissolved water and carbon dioxide in melt inclusions were measured using Fourier Transform Infrared Spectroscopy (FTIR)(Fine and Stolper, 1986; Ihinger et al., 1994). Melt inclusions were prepared as doubly polished wafers ranging in thickness from 25-200 μm. Transmission IR spectra were collected in the 1200-4000 cm^{-1} range using a Specta-Tech microscope attachment on a Nicolet Magna-IR 750 FTIR spectrometer. 512 scans of the sample and background were collected for each spectrum. Backgrounds of absorption peaks were drawn by hand. A flat background was used to determine the minimum peak height, and French curves were used to draw the preferred background. The difference between the background estimates was used as the error of the absorption peak height measurement. Absorption measurements of water were made using the fundamental O-H stretch peak at 3550 cm^{-1} which measures total water (hydroxyl and molecular water). Carbon dioxide was determined using the carbonate asymmetric stretch double peak near 1500 cm^{-1} and 1400 cm^{-1}. The carbonate concentration was calculated for each of the doublet peaks and then averaged. Quantification of the concentrations was done using the Beer-Lambert law (Appendix B). The thickness of the doubly polished wafers (melt inclusions) was measured using a Mitutoyo digital displacement micrometer which has a precision of ±1-2 μm. The glass

densities were calculated on a dry basis from the electron microprobe analyses of each sample following Lange and Carmichael (1987).

The molar absorptivities (proportionality constants between concentration and peak heights) are composition dependent and thus must be chosen appropriately. The molar absorptivity for the O-H stretching band at 3550 cm^{-1} has been shown not to be strongly compositionally dependent for basaltic compositions (Dixon et al., 1997). Therefore, a value of 63±5 for the basanite and phonotephrite samples was used. Carroll and Blank (1997) determined the extinction coefficients on experimentally charged phonolite samples for all water infrared peaks except 3550 cm^{-1}. Consequently, their sample Run129 was acquired and the extinction coefficient of 82.6±6.5 (2σ) was determined for the total water peak in phonolite. Dixon and Pan (1995) determined that the ratio of sodium to calcium in glass can be used to predict the molar absorptivity of carbonate in basaltic glasses. Their equation was used for all compositions in this study. This estimation is reasonable for the basanite and phonotephrite samples based on the compositions of the glasses used to develop the empirical equation. This equation may be less appropriate for the phonolite glasses. However, the molar absorptivity of carbonate in phonolite has not been determined, so the equation of Dixon and Pan (1995) is the best estimate at this time. All measured and calculated quantities are listed in Appendix B.

The uncertainty of the total H_2O and CO_2 analyses for most samples is ±11-12% and ±15% to ±50%, respectively. Some inclusions from the phonotephrite and tephriphonolite samples have estimated uncertainties of the H_2O analyses up to ±25%. The uncertainty of the carbonate determinations for the high concentration samples (DVDP 3-295, DVDP 3-283, 97009) is estimated at ±15%. The calculated uncertainties

are based on error propagation of the absorption peak height measurement, inclusion thickness, density, and molar absorptivity. Duplicate analyses of inclusions DVDP 3-283a and DVDP 3-283b indicate the reproducibility is better than ±2% for both water and carbonate.

Electron Microprobe

Concentrations of major elements as well as sulfur, fluorine and chlorine were determined on a Cameca SX-100 electron microprobe (Appendix C, D). The oxides of the major elements (Si, Al, Fe, Mn, Mg, Ca, P, K, Na, Ti) were determined for the melt inclusions and matrix glasses (where present). Glass analyses were conducted with a defocused beam of 15 to 25 μm in diameter depending on the size of the inclusion. A focussed beam of 1 μm diameter was used for all minerals except feldspar for which a 10 μm diameter beam was used. A beam current of 10 nA and accelerating potential of 15 kV was used for glasses while a current of 20 nA was used for mineral analyses.

The error for Cl and S analyses of glasses are around ± 200 ppm based on replicate analyses of standard glasses (Appendix H). Fluorine analyses have errors on the order of ± 1000 ppm.

Secondary Ion Mass Spectrometry

Trace elements were measured on selected melt inclusions using the Cameca 3f IMS at Arizona State University (Appendix E). Concentrations of the elements Li, B, Rb, Sr, Y, Zr, Ba, Th, Ce, Nd, Eu, Tb, and Tm were determined. Eu, Tb, and Tm were corrected for Ba, Nd, and Eu interferences respectively. A 2 nA primary beam of $^{16}O^-$

ions was focussed to a spot of 10-20 μm in diameter. Secondary ions were accelerated to +4500 eV. H was analyzed on 7 inclusions from sample DVDP 3-295 (Table E.2). Trace elements were calibrated against the standard NBS 610 and ^{30}Si was used for normalizing. The standard errors of the trace element analyses based on counting statistics are better than 5% for Li, F, Sr, Y, Zr, Nb, Ba, Ce, and <10% for B, Rb, Nd, and Tb. The elements Eu and Th have standard errors ≤15%. Tm has standard errors ≤24%. The interference corrections for Eu, Tb, and Tm are large and result in uncertainties much larger than the counting statistics estimate.

RESULTS

Melt Inclusions

Petrography

Large melt inclusions are abundant in olivine from all but the phonolite samples. The olivine-hosted melt inclusions in the phonolite are generally small and thus were not analyzed. The phonolite samples 97018 and EA1 are anorthoclase-hosted melt inclusions; all other samples are olivine-hosted melt inclusions. Olivine-hosted melt inclusions range in size from <20 to 350 μm. The inclusions are brown-colored transparent glass and have ovoid to negative crystal form often with cuspate boundaries (Figure 2 a,c). The inclusions are typically located throughout the crystals, with a slightly higher incidence in the corners of the crystals.

Melt inclusions in anorthoclase are generally very large; they range in size from <10 to >600 μm. The crystals contain both irregular and negative crystal form inclusions (Dunbar et al., 1994)(Figure 2d). Both types have angular boundaries.

Vapor bubbles are common within the inclusions. These bubbles comprise generally less than 1% of the inclusion volume, based on visual observation. It is common to find more than one vapor bubble within anorthoclase-hosted melt inclusions. In contrast to anorthoclase hosted melt inclusions, olivine-hosted melt inclusions typically contain at most one bubble, and many are bubble-free. Besides vapor bubbles, crystals commonly occur within the inclusions. Magnetite, apatite, and pyroxene crystals are all found in inclusions, however, generally only one mineral occurs within any one inclusion. Included magnetite crystals are typically small relative to the size of the inclusion (Figure 2a). However, apatite and pyroxene often make up a large percentage of the inclusion volume and appear to have caused the nucleation of the melt inclusion (Figure 2b). Iron sulfide globules occur in at least one inclusion from each sample. Typically, the sulfides are spherical and less than 3 μm in diameter, but can be as large as 30 μm occur in melt inclusions.

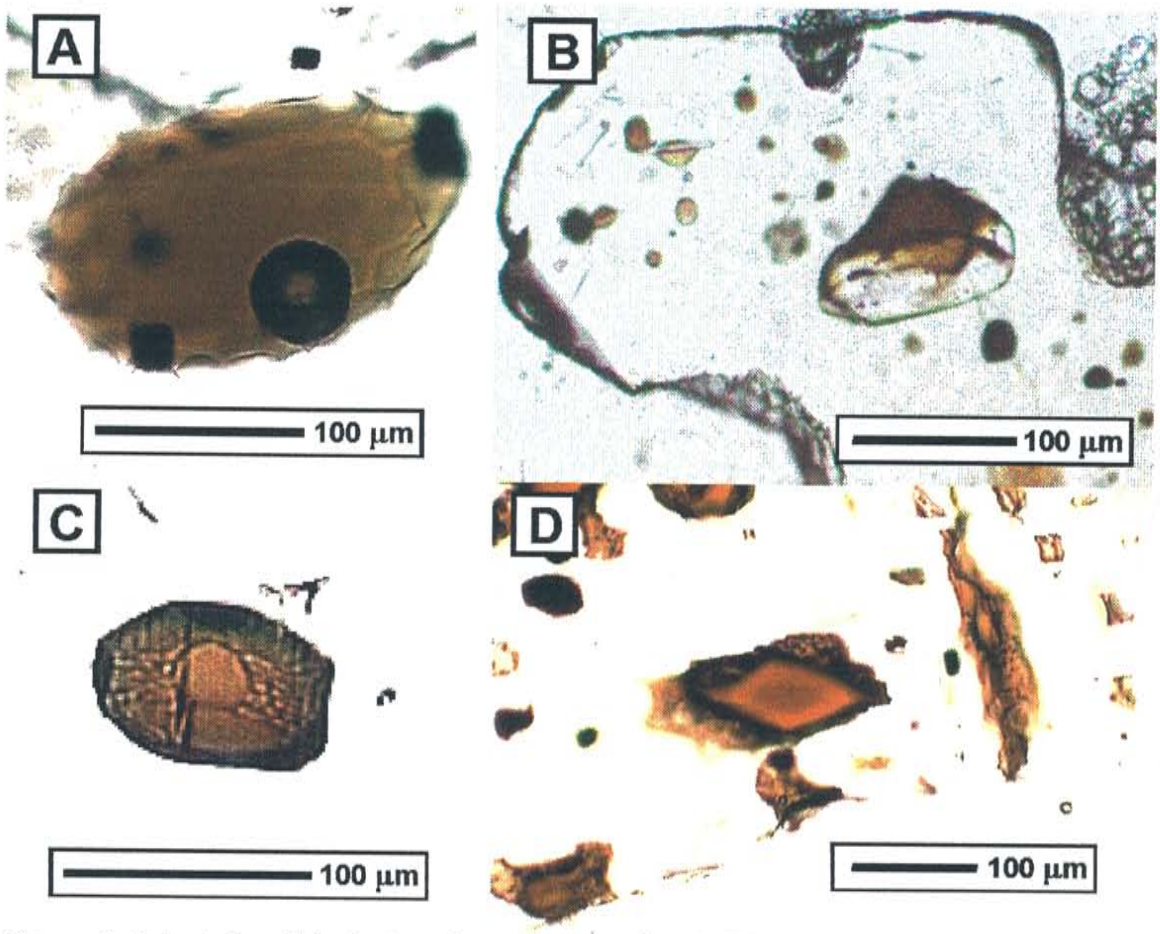

Figure 2. Selected melt inclusion photomicrographs. A. DVDP 3-283c (basanite) The dark spots in the lower left and upper right corners are magnetite crystals. B. AW82033I (phonotephrite) Melt inclusion trapped adjacent to an apatite crystal. C. 97010c (tephriphonolite) Negative crystal form inclusion in olivine. D. EA1h (phonolite) Negative crystal and irregular form melt inclusions in anorthoclase.

Major Elements

Table 1 gives the mean electron probe, FTIR, and ion probe analyses of the melt inclusions from each sample. Figure 3a shows melt inclusion compositions plotted on the total alkali versus silica chemical classification scheme of Le Bas et al., 1986. This diagram shows the continuous chemical trend of the melt inclusions from basanite to phonolite. Figure 3b shows the melt inclusion compositions (fields) in comparison to

bulk rock compositions (Appendix C, F). The difference between the melt inclusion compositions and the bulk rock compositions is due to sample mineralogy. For example, anorthoclase crystals in phonolite cause the melt inclusion compositions to shift away from the trachyandesite field relative to the bulk rock.

The major element compositions of melt inclusions and matrix glasses are very similar in most cases (Appendix C). Common deviations include small depletions in S, MgO, CaO and enrichments in K_2O, and Na_2O in the matrix glass. The sulfur depletion can be attributed to degassing during/following eruption. Both the enrichments in the alkali elements and the depletions in the alkaline earth elements are explained by fractionation of the matrix during cooling, as most of the glasses contain microphenocrysts of pyroxene. Samples without abundant microphenocrysts (i.e. 97018) show extremely good agreement between melt inclusion and matrix glass composition.

Table 1. Major, Volatile, and Trace Element Chemistry of Melt Inclusions

Sample	DVDP 3-295	DVDP 3-283	AW82033	7713	97009	97010	97011	97006	97018	EA1
Electron Microprobe Analyses										
	n=10	n=4	n=11	n=8	n=10	n=6	n=6	n=4	n=7	n=10
SiO_2	41.03 (1.10)	41.85 (1.34)	44.75 (1.76)	47.72 (0.39)	51.11 (1.61)	53.56 (0.62)	53.77 (1.15)	54.46 (0.54)	55.64 (0.88)	54.83 (0.60)
TiO_2	4.14 (0.15)	4.17 (0.18)	3.56 (0.55)	2.70 (0.17)	1.82 (0.17)	1.87 (0.17)	1.34 (0.14)	1.35 (0.07)	0.96 (0.09)	0.95 (0.04)
Al_2O_3	14.56 (0.57)	14.10 (0.48)	17.36 (0.85)	17.81 (0.31)	19.28 (0.47)	19.63 (0.54)	20.07 (0.32)	19.68 (0.11)	20.16 (0.49)	19.79 (0.28)
FeO_T	10.26 (0.96)	10.33 (1.58)	10.83 (1.02)	10.43 (0.28)	7.17 (0.40)	6.71 (0.49)	5.43 (0.21)	5.78 (0.16)	5.38 (0.22)	4.98 (0.10)
MnO	0.16 (0.02)	0.19 (0.01)	0.23 (0.06)	0.25 (0.03)	0.20 (0.02)	0.19 (0.02)	0.20 (0.05)	0.21 (0.01)	0.27 (0.05)	0.25 (0.03)
MgO	5.85 (0.24)	5.85 (0.43)	3.59 (0.45)	2.31 (0.29)	1.31 (0.10)	1.21 (0.11)	0.89 (0.06)	0.90 (0.06)	0.84 (0.03)	0.81 (0.03)
CaO	12.85 (0.98)	13.74 (0.39)	9.43 (1.69)	6.71 (0.32)	3.97 (0.34)	3.56 (0.19)	3.08 (0.27)	2.40 (0.19)	1.92 (0.10)	1.81 (0.12)
Na_2O	3.69 (0.31)	3.53 (0.46)	5.03 (0.51)	6.21 (0.63)	7.65 (0.44)	8.01 (0.35)	8.16 (0.39)	8.57 (0.24)	8.98 (0.27)	8.82 (0.27)
K_2O	1.63 (0.13)	1.54 (0.14)	2.43 (0.78)	3.49 (0.07)	4.90 (0.13)	5.22 (0.12)	5.58 (0.18)	5.36 (0.08)	5.64 (0.13)	6.29 (0.27)
P_2O_5	0.92 (0.07)	0.78 (0.09)	1.31 (0.28)	1.30 (0.15)	0.55 (0.10)	0.77 (0.11)	0.58 (0.18)	0.49 (0.11)	0.30 (0.05)	0.30 (0.02)
F (ppm)	1572 (325)	1978 (228)	2133 (713)	2774 (480)	1386 (859)	2406 (672)	2035 (363)	1973 (725)	2254 (513)	2652 (347)
S (ppm)	2166 (228)	2036 (114)	1330 (244)	1109 (247)	671 (131)	616 (157)	628 (145)	658 (185)	367 (131)	375 (58)
Cl (ppm)	875 (175)	740 (122)	784 (182)	1038 (170)	2172 (2053)	1223 (154)	1352 (144)	1325 (135)	1457 (163)	1502 (171)
Total	95.55 (1.82)	96.56 (1.04)	98.94 (1.65)	99.42 (0.94)	98.39 (2.55)	101.14 (0.57)	99.51 (1.61)	99.58 (0.55)	100.50 (1.55)	99.27 (1.11)
Fourier Tranform Infrared Analyses										
CO_2 (ppm)	5520 (973)	5648 (815)	825 (623)	448 (149)	2421 (707)	877 (507)	1118 (587)	1166 (367)	650 (139)	690 (125)
H_2O (wt%)	1.50 (0.19)	1.41 (0.24)	0.16 (0.07)	0.11 (0.02)	0.53 (0.07)	0.12 (0.01)	0.10 (0.02)	0.08 (0.01)	0.12 (0.05)	0.17 (0.02)

Table 1. Continued. Trace Element Chemistry of Melt Inclusions

Sample	DVDP 3-295	DVDP 3-283	AW82033	7713	97009	97010	97011	97006	97018	EA1
Ion Microprobe Analyses*										
	n=8		n=4	n=4	n=4	n=4	n=2	n=2	n=3	
Li	7.2 (1.2)		9.4 (4.0)	14.7 (0.7)	23.6 (1.8)	23.9 (1.9)	29.4 (0.8)	29.9 (3.2)	41.8 (2.6)	
B	5.7 (1.3)		5.9 (1.3)	9.3 (3.0)	10.4 (0.5)	11.5 (0.7)	13.0 (0.4)	15.3 (0.4)	17.0 (1.6)	
F	1935 (138)		1728 (520)	2466 (354)	2202 (372)	2234 (398)	2240 (207)	2337 (414)	2425 (328)	
Rb	38 (2)		46 (12)	64 (6)	89 (8)	102 (12)	103 (6)	120 (3)	123 (9)	
Sr	1005 (23)		947 (255)	924 (49)	681 (22)	571 (56)	516 (90)	308 (7)	280 (8)	
Y	38 (2)		46 (16)	49 (5)	41 (2)	47 (2)	45 (3)	55 (0.2)	62 (1)	
Zr	467 (22)		516 (97)	647 (33)	832 (19)	986 (41)	1055 (36)	1270 (6)	1475 (129)	
Nb	103 (4)		134 (42)	191 (21)	263 (12)	268 (15)	276 (18)	318 (10)	391 (44)	
Ba	540 (39)		678 (132)	950 (122)	1064 (40)	950 (51)	1013 (8)	724 (36)	675 (84)	
Ce	161 (6)		244 (112)	243 (34)	226 (16)	255 (17)	239 (21)	275 (13)	326 (54)	
Nd	70 (4)		94 (35)	86 (15)	73 (3)	86 (5)	71 (2)	89 (6)	99 (17)	
Eu	3.3 (0.5)		4.6 (1.7)	4.9 (0.5)	3.5 (0.9)	4.6 (0.3)	2.7 (0.4)	3.6 (0.1)	4.0 (0.7)	
Tb	1.8 (0.4)		2.2 (0.8)	2.1 (0.2)	2.0 (0.2)	2.4 (0.4)	2.1 (0.5)	2.8 (0.2)	3.5 (0.2)	
Tm	0.7 (0.1)		0.9 (0.3)	1.0 (0.3)	0.9 (0.3)	0.9 (0.4)	1.1 (0.1)	1.0 (0.1)	1.5 (0.2)	
Th	9.2 (1.1)		12.8 (4.5)	16.2 (3.0)	22.7 (2.6)	24.8 (4.1)	28.2 (4.7)	27.7 (1.0)	39.0 (8.2)	

n – number of analyses. All inclusions analyzed by electron probe were analyzed by FTIR.

* Ion microprobe analyses expressed in ppm. Numbers in parentheses represent one standard deviation.

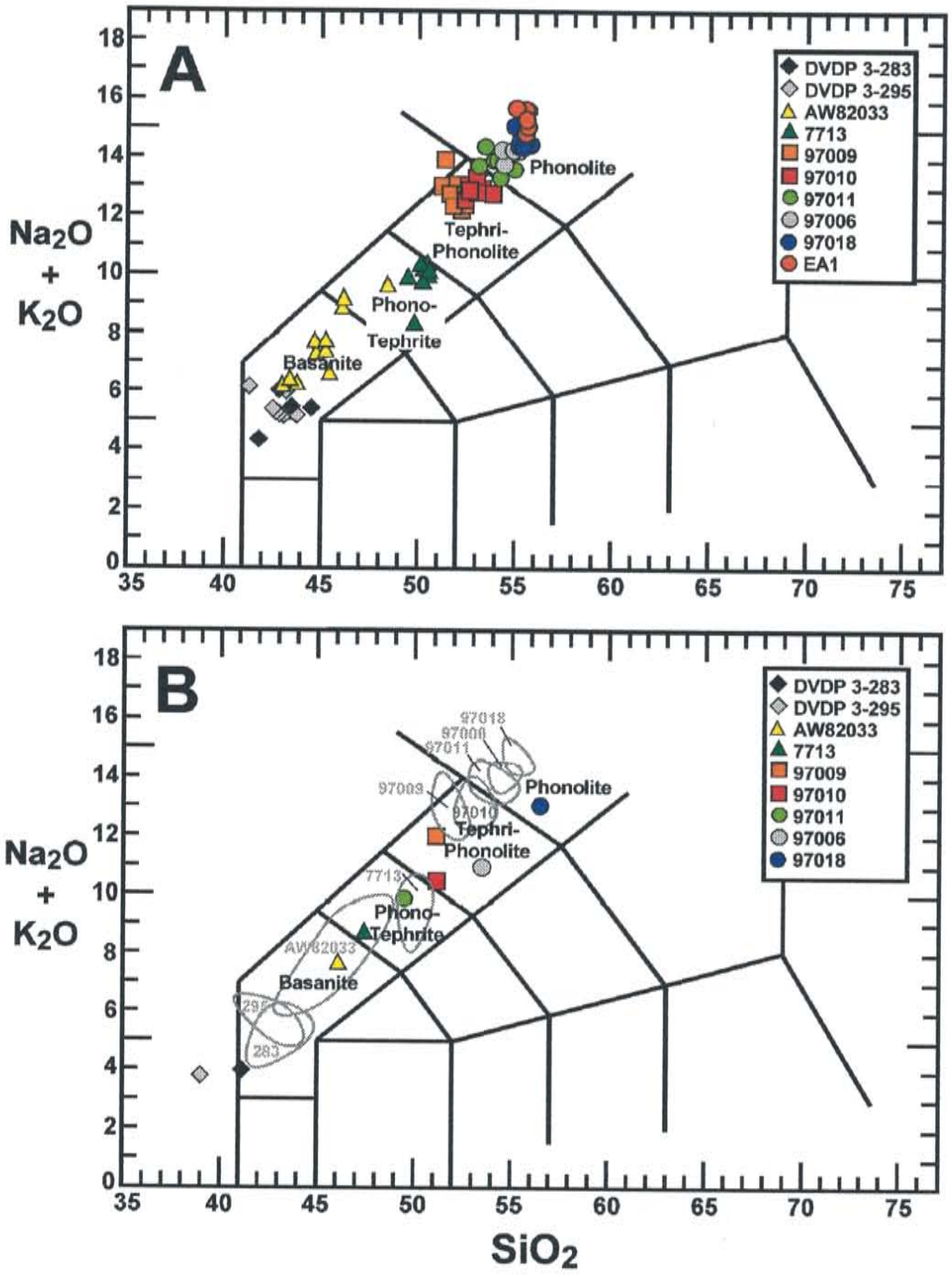

Figure 3. Total alkali versus silica diagrams for: A. Analyses of melt inclusions. B. Color symbols indicate bulk rock analyses with melt inclusion compositions (fields). Sample EA1 is a single anorthoclase crystal, therefore, it does not have a corresponding whole rock analysis. Classification after Le Bas et al. (1986).

Trace Elements

Average trace element compositions of analyzed melt inclusions are listed in Table 1 (individual analyses are given in Table E.1.). The trace element results are shown in a series of graphs with Li, B, Rb, Sr, Y, Zr, Ba, Ce, and Th plotted against Nb (Figure 4). Nb is used for comparison because of its highly incompatible nature. The concentrations of the elements Li, B, Rb, Zr, Th, and Nb exhibit a factor of four increase through the compositional range of samples (Figure 4a-c, f, i). This increase indicates the elements are behaving as incompatible elements, and is consistent with the magnitude of fractional crystallization modeled for the sequence (Kyle et al., 1992). Yttrium and the rare earth elements increase in concentration with magma evolution, though not at the magnitude suggested by fractional crystallization (Figure 4e, h). This suggests that these elements are partitioned into a mineral phase (pyroxene and apatite). Ba content increases from the primitive basanites to phonotephrite. Following the phonotephrites the Ba content decreases, this decrease is coincident with the appearance of feldspar suggesting that Ba is partitioned into feldspar. Sr acts as a compatible element and decreases with fractional crystallization (Figure 4d).

The fields of bulk rock analyses of Kyle et al. (1992) generally overlap with the trends of the melt inclusion data. The conspicuous difference between these data sets is that the Nb contents of the bulk rock data only covers a small portion of the range exhibited by the melt inclusions. The melt inclusion data extend through the trend of the bulk rock data. The bulk rock analyses from this study (Appendix F) are similar to those of Kyle et al. (1992).

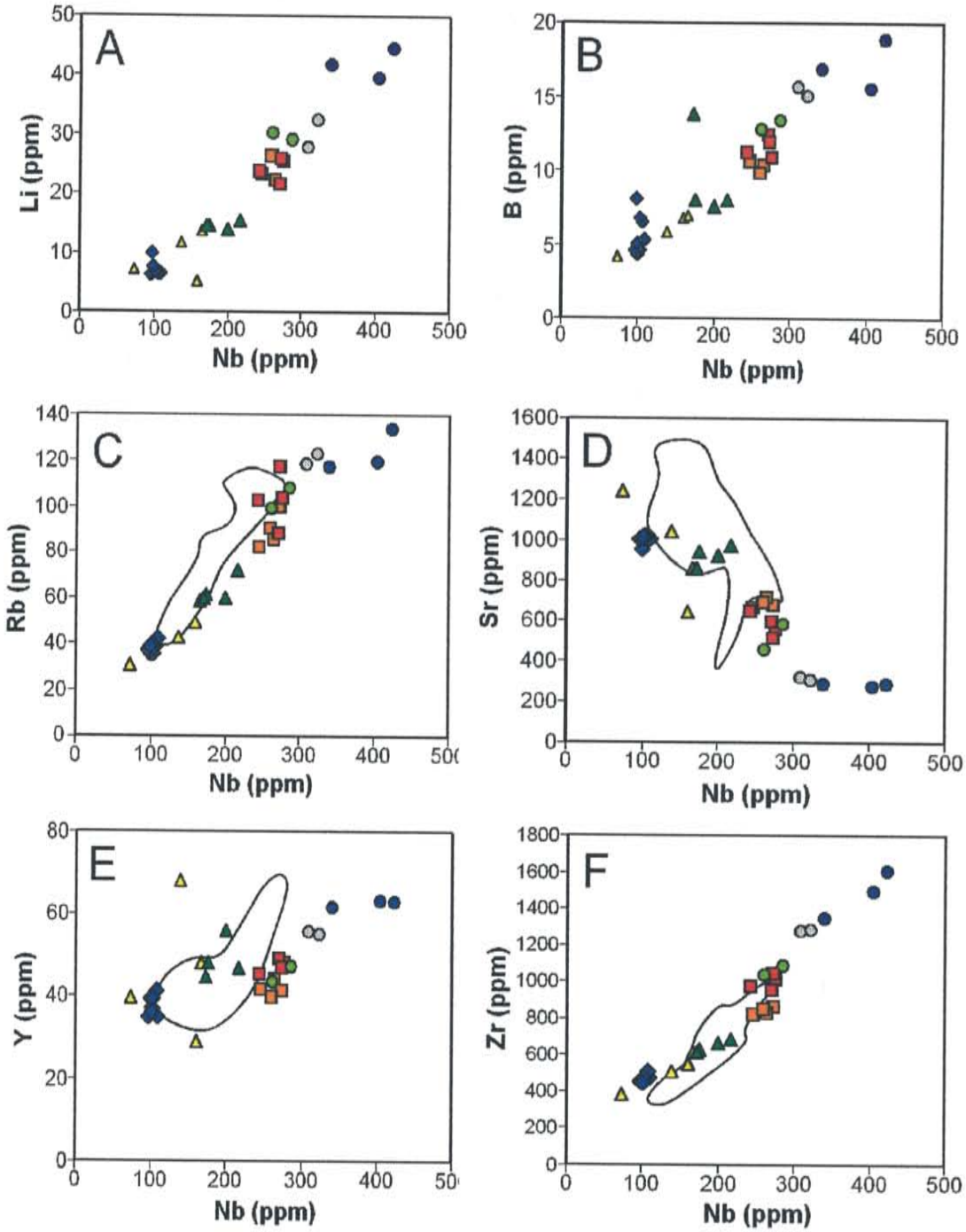

Figure 4. Plots of trace element contents of analyzed melt inclusions. Fields indicate bulk rock compositions of Erebus Lineage samples of Kyle et al., (1992). A. Li versus Nb. B. B versus Nb. C. Rb versus Nb. D. Sr versus Nb. E. Y versus Nb. F. Zr versus Nb.

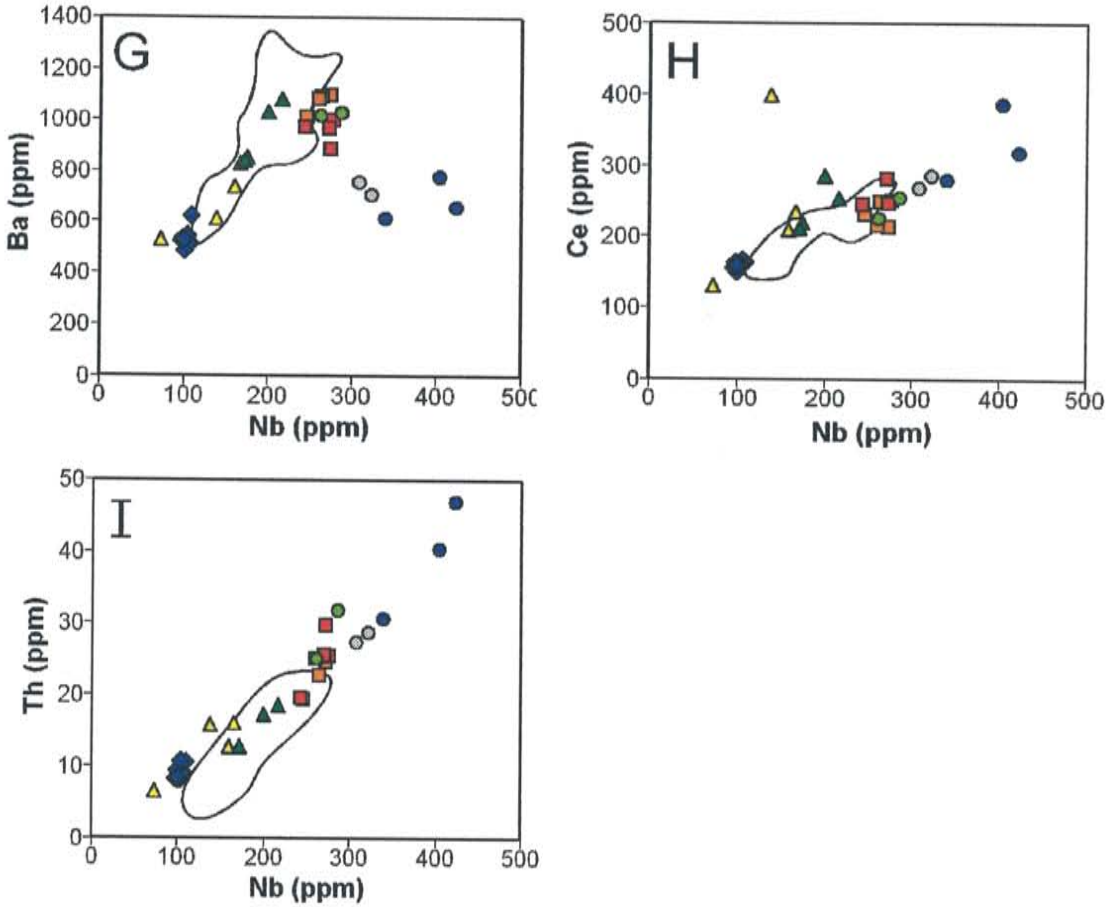

Figure 4. Continued. Plots of trace element contents of analyzed melt inclusions. G. Ba versus Nb. H. Ce versus Nb. I. Th versus Nb.

Mineral Chemistry

Olivine

Olivine is ubiquitous throughout the compositional range of magmas from Mount Erebus. Melt inclusion-bearing olivine crystals are euhedral and unzoned. Rare compositionally zoned olivine crystals are found in the basanites. These crystals almost never contain sizable melt inclusions, and appear to be xenocrysts. The olivines varies regularly with magma composition from ~Fo85 in the basanites to ~Fo52 in phonolite (Table 2).

Table 2. Mean Forsterite Content of Olivine

Sample*	MI SiO_2	Fo content (%)	Standard Deviation	N
DVDP3-295	41.03	84.4	2.4	6
DVDP3-283	41.95	84.5	2.1	17
AW82033	44.75	75.9	5.4	9
7713	47.72	65.1	0.6	9
97009	51.11	59.9	0.4	9
97010	53.56	63.0	1.3	9
97011	53.77	61.5	1.5	6
97006	54.46	55.7	0.6	4
97018	55.64	52.2	0.3	10

* Samples listed in order of increasing mean melt inclusion SiO_2.
N - number of analyses.

Pyroxene

Pyroxene is ubiquitous in Erebus lavas. Their compositions are as follows: Wo 45-51%, En 34-44%, Fs 8-20%, and plot within the diopside field (Figure 5) (Morimoto, 1989). The Wo and En components decrease with magma fractionation while the Fs component increases. Only the basanite samples have pyroxenes with significant zonation.

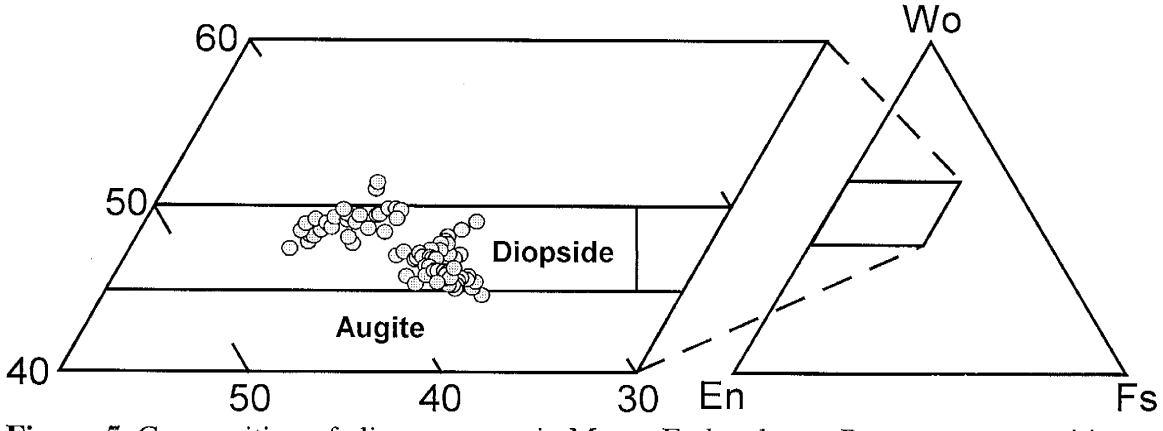

Figure 5. Composition of clinopyroxene in Mount Erebus lavas. Pyroxene compositions plotted in terms of calculated wollastonite, enstatite, and ferrosillite end-member components.

Feldspar

Plagioclase is abundant in phonotephrite samples (AW82033, 7713) and present as a minor component in tephriphonolite samples (97009, 97010). The plagioclase in the phonotephrites are: Ab 37-47%, An 49-60%, Or 3-5% (Figure 6).

Anorthoclase phenocrysts are characteristic of the Mount Erebus phonolite lavas. These large crystals (up to 9 cm) have as much as 30 vol% MI (Dunbar et al., 1994). The crystals show numerous growth zones that are emphasized by inclusion rich zones. The Ab component of the crystals varies little (Ab = 66-67%), while An and Or components vary considerably more (Figure 6). The crystals from a bomb erupted in 1997 (97018) have An and Or contents of 16-18% and 16-19% respectively. A single crystal from an older bomb (EA1) has contents of An = 18-21% and Or = 13-16%. These ranges in composition are comparable with those of single crystal zonation found by Kyle (1977) and Dunbar et al., (1994).

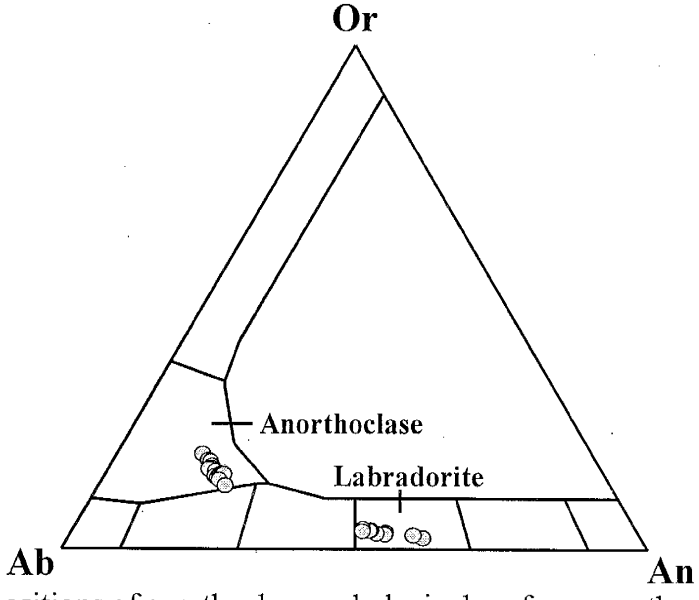

Figure 6. Compositions of anorthoclase and plagioclase from anorthoclase phonolites and phonotephrites respectively. Ternary diagram plotted with calculated albite, anorthite and orthoclase end-member components.

Apatite

Apatite occurs as hexagonal, acicular crystals in the phonotephrite, tephriphonolite, and phonolite samples. Only those crystals within melt inclusions were analyzed by electron microprobe. These analyses are listed in Table D.5. (Appendix D). The apatite generally contains 4-5.5 wt% F and 0.2 wt% Cl.

Magnetite

Magnetite occurs throughout the compositional range of samples. Magnetite analyses are listed in Table D.4. (Appendix D). The magnetites are chromium- and aluminum-rich in the basanite samples, and titanium-rich in all other samples. Magnetite grains in melt inclusions were the only crystals analyzed.

Volatiles

Water

Water concentrations in melt inclusions show considerable variation with an overall decrease in concentration from basanite to phonolite (Table 1) (Figure 7). The silica content of the inclusions is used as a proxy for degree of fractional crystallization. However, the silica content does not vary linearly with fractional crystallization, therefore the degree of fractionation (percent crystallization of the parental basanite) is also plotted on Figures 7-11. The degree of fractionation was determined by correlating the MI silica content with the model compositions of Kyle et al., (1992). The average concentration of water in DVDP basanite MI is 1.5 wt%. The water concentrations range from 1.15 to 1.75 wt%. This range is most likely due differences in depth of inclusion entrapment as well as analytical uncertainty.

The H_2O concentrations of MI in the more evolved compositions are dramatically lower than those in basanite. With the exception of sample 97009, the inclusions from phonotephrite through phonolite have water concentrations near 0.1 wt%. Inclusions from sample 97009 contain an average 0.5 wt% water. The samples with low water contents exhibit remarkable similarity and have saturation pressures on the order of tens of bars.

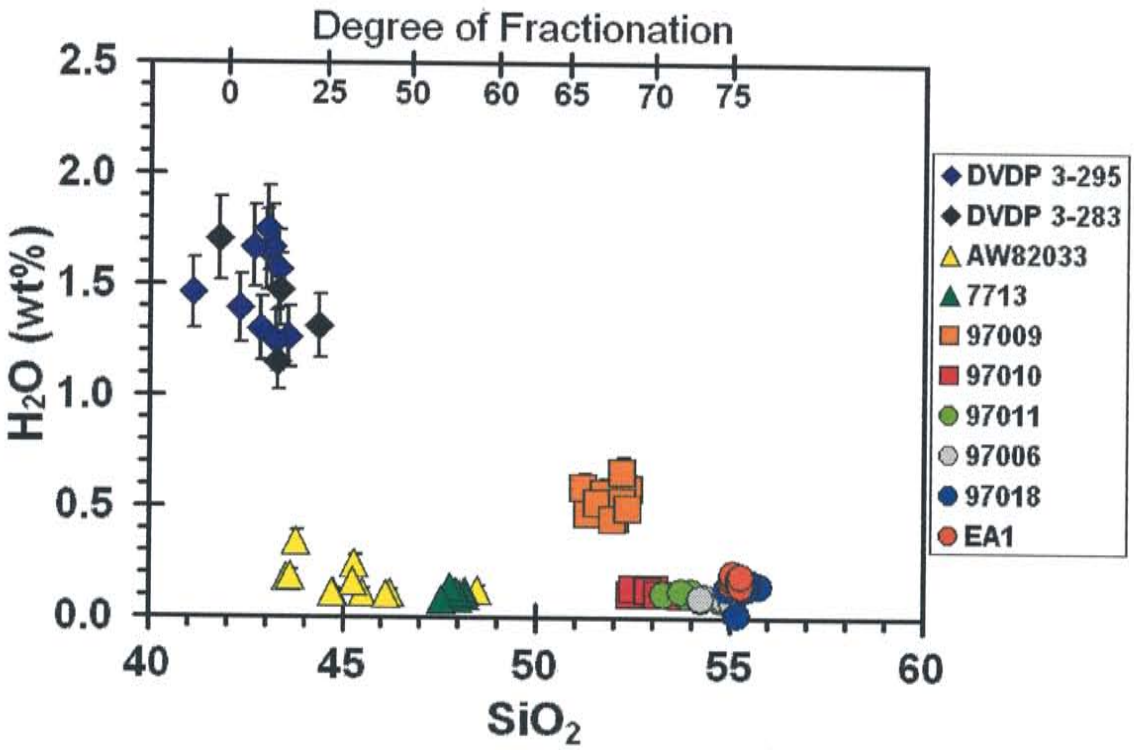

Figure 7. Melt inclusion water content versus SiO_2. Error bars represent 2σ uncertainty. Degree of fractionation expressed as % crystallization of the parental basanite.

Carbon Dioxide

Carbon dioxide concentrations in DVDP basanite MI range from 4000-7300 ppm (Table C.1.) (Figure 8). The tephriphonolite sample, 97009, has concentrations ranging from 1500-3600 ppm CO_2. Most other inclusions have CO_2 concentration less than 2000 ppm and generally less than 1000 ppm. These low CO_2 samples correlate directly with the low water samples. The dramatic decrease in CO_2 with fractional crystallization is consistent with the general compositional dependence of CO_2 solubility (decrease) with increasing SiO_2 (Blank and Brooker, 1994).

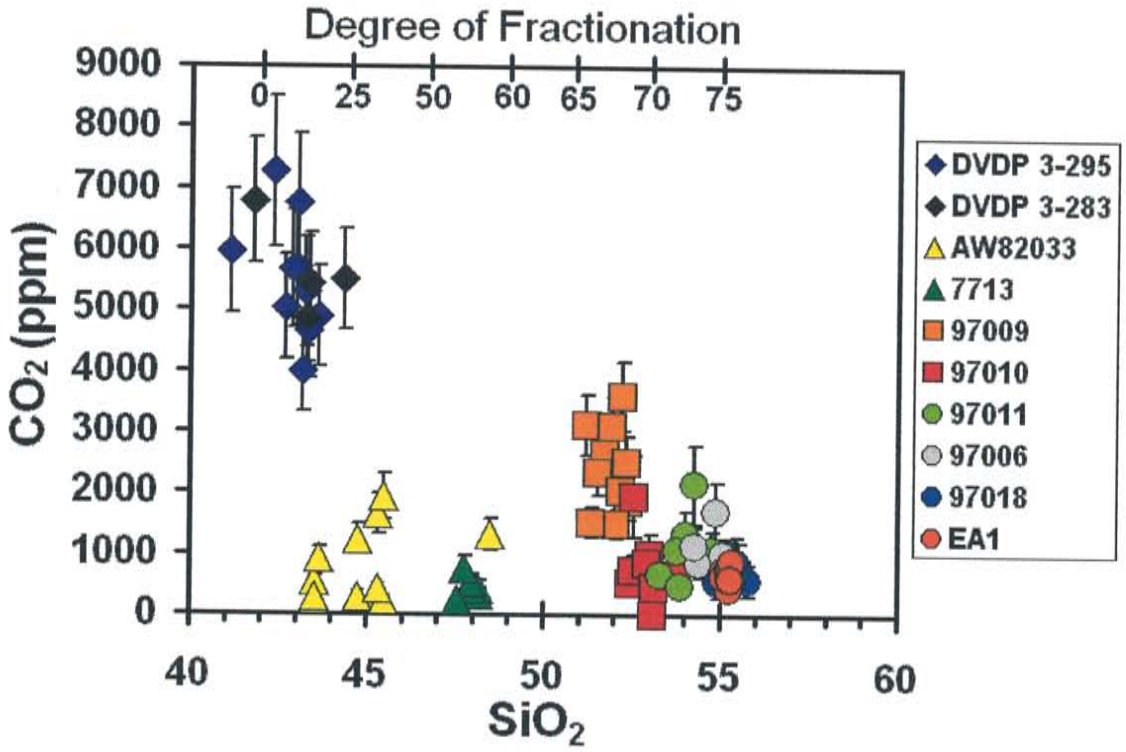

Figure 8. Melt inclusion CO_2 content versus SiO_2. Error bars represent 2σ uncertainty. Degree of fractionation expressed as % crystallization of the parental basanite.

Sulfur

Dissolved sulfur concentrations exhibit a decreasing trend from values of ~2500 ppm in basanite to <500 ppm in phonolite (Table 1) (Figure 6a). Sulfide globules are present in inclusions from all samples, which indicate that all of the samples are saturated with respect to sulfide. The sulfur contents of phonolite through phonotephrite show a linear relationship with FeO (Figure 6b). However, the sulfur content of the basanite is higher than that of the phonotephrite although the FeO contents are similar. This indicates that sulfur solubility is enhanced in the basanite.

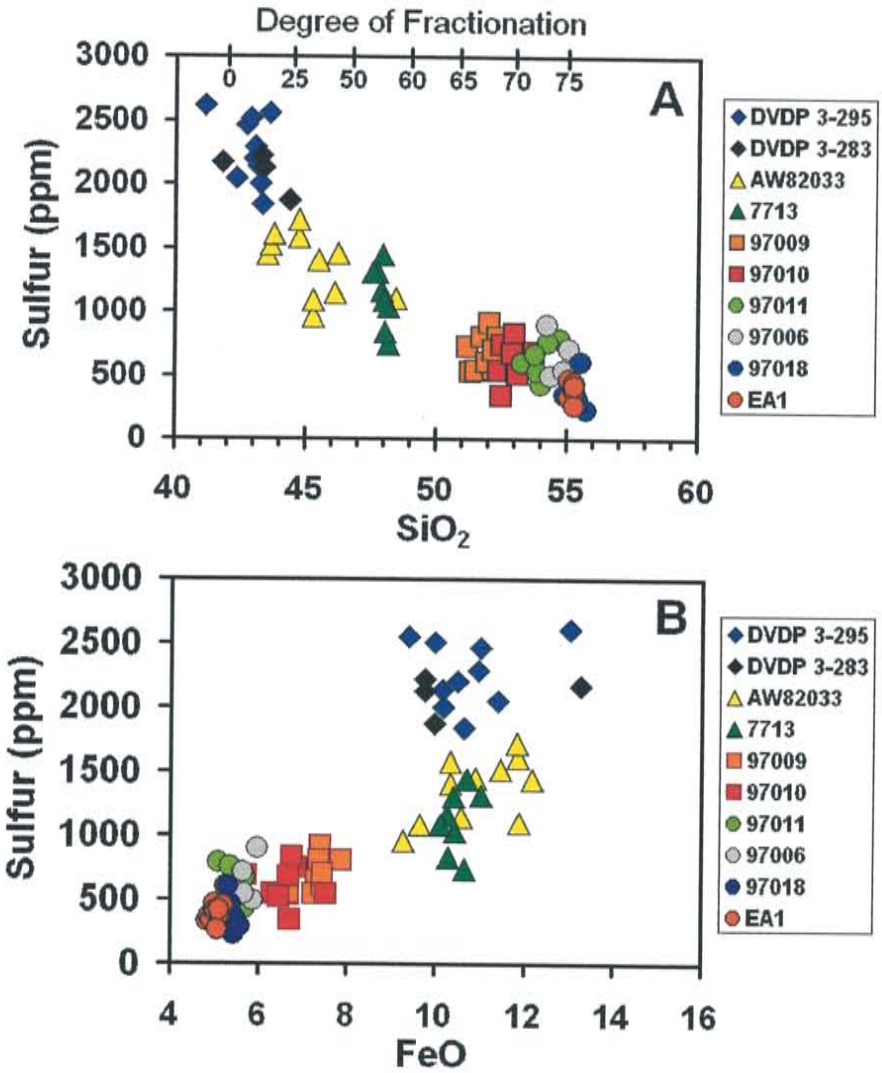

Figure 9. Melt inclusion sulfur contents (ppm) versus SiO_2 (A) and FeO (B)

Fluorine

There is little change in fluorine concentrations throughout the range in inclusion composition (Figure 10). Mean fluorine concentrations range from 1600 ppm to 2600 ppm. There is a slight increase in concentration from basanite through the phonotephrite samples (AW82033, 7713). This trend does not continue in any recognizable form past the phonotephrites. In fact, the fluorine concentrations are generally lower than sample 7713 in the more evolved samples. The decrease in concentration at this point can be attributed to both degassing and removal of fluorine by apatite crystallization.

The increase from basanite through the phonotephrite samples is consistent with fluorine increasing as an incompatible element during early stages of fractional crystallization.

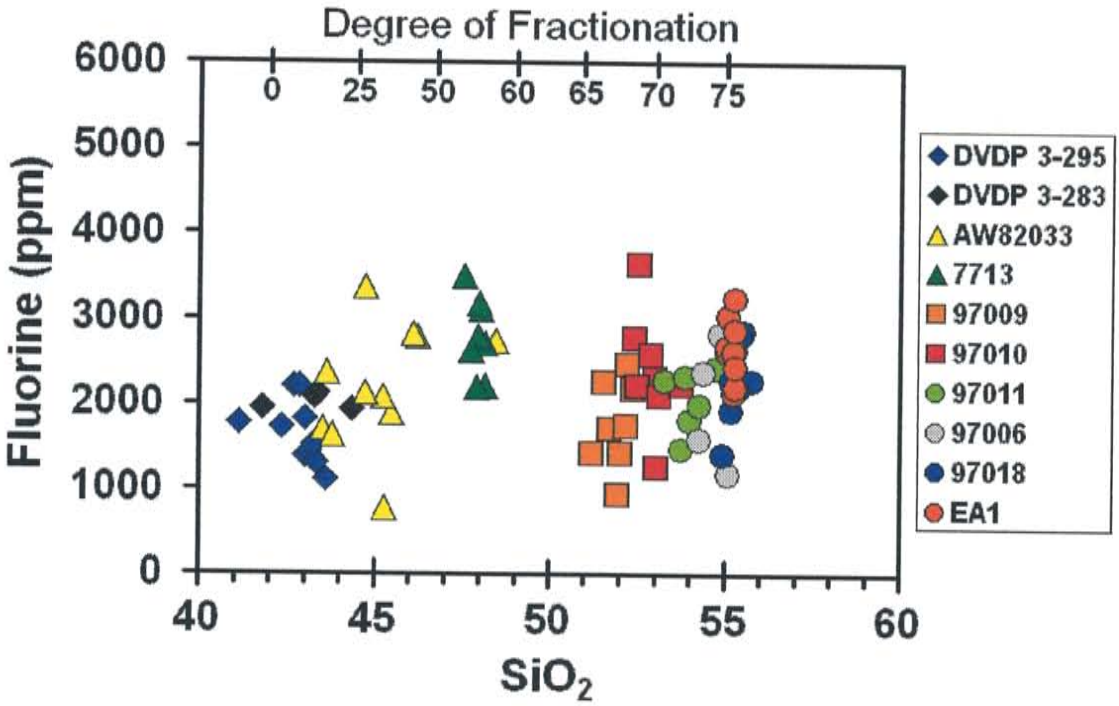

Figure 10. Melt inclusion fluorine contents versus SiO_2. Degree of fractionation expressed as % crystallization of the parental basanite.

Chlorine

Chlorine exhibits a trend of increasing concentration with fractional crystallization (Figure 11). Chlorine concentrations range from about 800 ppm in basanite to ~1500 ppm in phonolite. The concentration increase with magma evolution is less than would be expected if chlorine behaved as an incompatible element during fractional crystallization. This suggests that a small fraction of the chlorine is lost continuously during fractional crystallization. This loss is most likely due to degassing as the apatite contains very little chlorine and its crystallization would not cause significant loss.

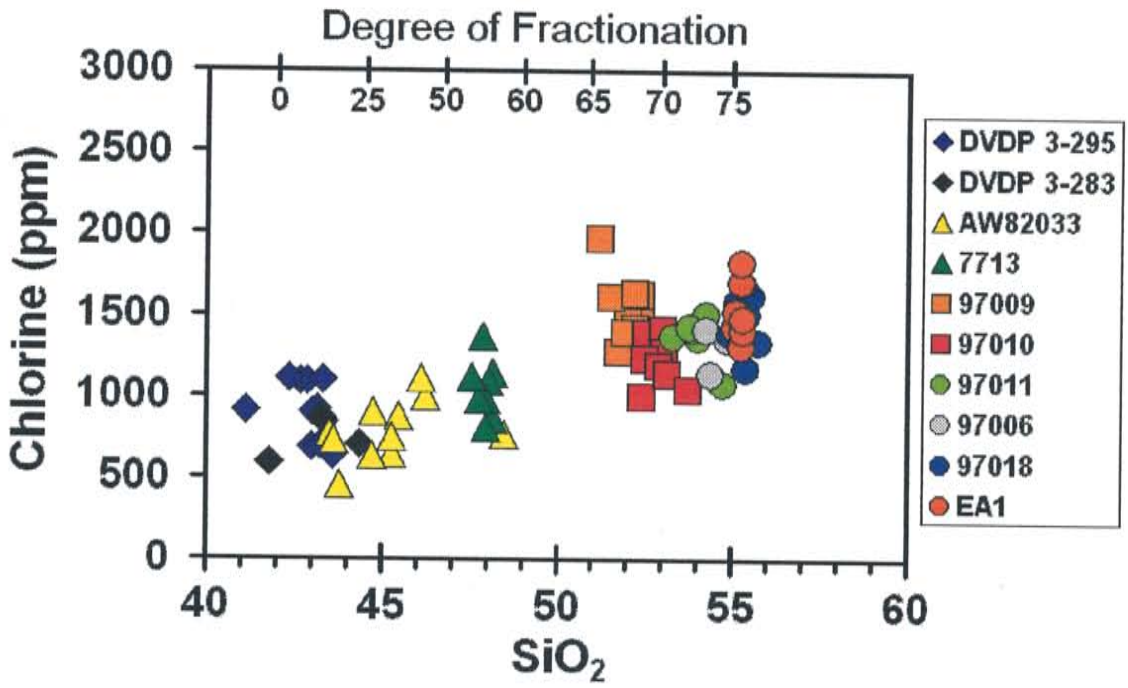

Figure 11. Melt inclusion chlorine content versus SiO_2. Degree of fractionation expressed as % crystallization of the parental basanite.

DISCUSSION

Sulfur

Experimental studies have shown that FeO_T content of a melt strongly influences the solubility of sulfur (Poulson and Ohmoto, 1990; Carroll and Webster, 1994). The strong correlation of sulfur contents of melt inclusions with Fe content supports these findings. There is a strong positive correlation between S and FeO with the exception of samples DVDP 3-283 and DVDP 3-295, which have similar FeO contents to samples AW82033 and 7713 but higher sulfur contents. This suggests that sulfur solubility is enhanced in these samples by some other factor. However, the concentration of sulfur in the basanite melt inclusions (up to 2600 ppm) is similar to sulfur solubilities determined for basaltic magmas (Wendlandt, 1982; Wallace and Carmichael, 1992).

Sulfur solubility is proportional to $(f_{S_2})^{1/2}$, $(f_{O_2})^{-1/2}$, and has a strong positive dependence on temperature (Wendlandt, 1982; Poulson and Ohmoto, 1990). There is also a general compositional control on sulfur solubility. Sulfur solubility increases with increasing mole fraction of the oxides: SiO_2<MgO<CaO<MnO≈FeO; SiO_2<Na_2O; and SiO_2<Al_2O_3 (Poulson and Ohmoto, 1990). This relationship suggests Mn, Ca, and Mg as well as Fe exert control on sulfur solubility. The pressure dependence of sulfur solubility is small, and has been found to be positive or negative depending on the experimental melt composition and pressure range (Carroll and Webster, 1994; Wendlandt, 1982).

Sulfide-globule-bearing MI exist in all samples. This is clear indication that all magmas were saturated with respect to sulfide and were under reducing conditions (near the FMQ buffer or lower).

The enhanced sulfur solubility of the DVDP basanites over the samples AW82033 and 7713 suggests other factors besides Fe content are important. The presence of sulfide globules throughout the range of melts suggest that oxygen fugacity has not changed significantly throughout fractional crystallization. The correlation between the higher concentrations of sulfur, H_2O and CO_2 in the DVDP basanite relative to the other compositions indicates that pressure may effect the solubility of sulfur in the Mount Erebus lavas. This relationship could also suggest that sulfur was scavenged by degassing of H_2O and/or CO_2 in the more evolved compositions. The solubility enhancement in basanite is likely due to the bulk composition of the melt as well as the physical conditions of the magma that existed during MI trapping such as temperature, pressure and degassing.

More importantly, the decreasing trend in sulfur concentration with magma fractionation shows that sulfur is lost (degassed) and not conserved as its overall concentration increases as an incompatible element. The amount of Fe-sulfide in the lavas is very small, therefore the sulfide phase is probably not a sink for significant amounts of the lost sulfur. The sulfur concentration decreases throughout the compositional range of the magmas indicating that sulfur is degassing continuously throughout magma fractionation.

Fluorine and Chlorine

The variations of Cl and F as a function of magmatic evolution indicate the halogens do not behave completely incompatibly during fractional crystallization. The magnitude of the concentration increase with magma evolution indicates the halogens

degas throughout fractional crystallization. Little is known about the solubility relationships of the halogens. Their solubilities, especially that of Cl, probably are strongly effected by the presence of a water-bearing vapor phase. An aqueous fluid or vapor can distill Cl out of magmas during degassing because Cl preferentially partitions into the water-bearing phase (Anderson, 1974; Carroll and Webster, 1994). Solubility of Cl^- varies directly with pressure and molar ((Al+Na+Ca+Mg)/Si) ratio and inversely with H_2O content (Webster et al., in press). Experimental studies have shown than H_2O-deficient basalts must contain at least 2 wt% Cl before a Cl^- enriched volatile phase will exsolve (Webster et al., in press). This suggests that Cl loss in the Mount Erebus magmas is caused by distillation by a water-bearing vapor phase.

Very little work has been done to address the solubility of fluorine in basic magmas. In general, F solubility varies inversely with a_{SiO_2} and directly with the alkaline earth elements (Carroll and Webster, 1994). F is relatively soluble in magmas, generally less than or equal to the water solubility. The fluorine concentrations indicate that the loss may be due to a distillation mechanism similar to chlorine. Fluorine is also removed from the system by crystallization of apatite.

Water

The MI H_2O concentrations of different melt compositions are not consistent with a simple explanation involving magmatic processes. The H_2O content of MI in basanite is high, but the more evolved samples have generally low water contents. These variations are paradoxical and suggest that water is not behaving as a simple incompatible element during magmatic differentiation.

If the DVDP basanites are representative of the parental magma, the phonotephrite MI would be expected to have much higher H_2O concentrations than is observed due to fractionation and the incompatible nature of H_2O. The calculated solubility H_2O for the range of observed compositions for a given pressure does not vary significantly (Figure 12). When phonotephrite is produced by fractional crystallization of basanite, the water content of the melt would be expected to increase, but the pressure may decrease somewhat due to the magma body being higher in the crust. If the basanite was near saturation with respect to H_2O, the phonotephrite may contain slightly less water than the basanite due to the decrease in pressure. As a function of the decrease in pressure, the magma will be oversaturated and will exsolve water (degas).

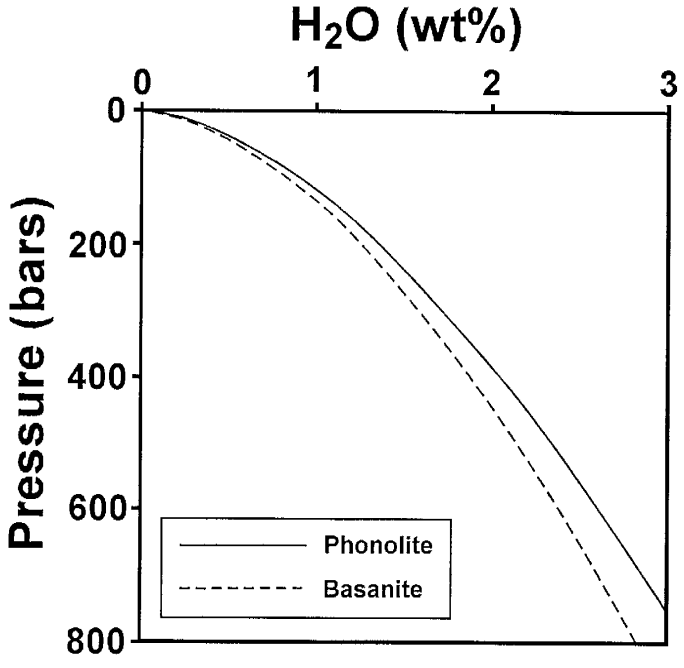

Figure 12. Water solubility curves modeled for basanite at 1200°C (dashes) and phonolite at 1000°C (solid line). Intermediate compositions range in between the two curves. Solubilities modeled after Moore et al., (1998).

The scenario outlined above is clearly not the observed situation. Most of the samples contain low-water concentrations melt inclusions, i.e. AW82033, 7713, 97010, 97011, 97006, 97018 and EA1. The saturation pressures of these melt inclusions are all less than 20 bars and typically less than 10 bars assuming water is the only volatile phase present (Moore et al. 1998). The volatile contents of the intermediate composition samples should be higher if the magmas resided at substantial depths and were formed from a parental magma similar to the basanite.

The simplest explanation for the low water concentration MI is that they represent magma trapped in shallow magma chambers (low pressure). This suggests that the crystals that have trapped the melt inclusions are not the crystals that have caused the fractional crystallization but have grown later in the history of the magma after the magma was emplaced in a shallow chamber.

Carbon Dioxide

The CO_2 contents of the DVDP basanite melt inclusions (4000-7300 ppm) are extraordinarily high. Numerous studies have measured CO_2 contents of basaltic melt inclusions (Metrich and Clocchiatti, 1989; Metrich et al., 1991; Anderson and Brown, 1993; Roggensack et al., 1997) and submarine matrix glasses (Fine and Stolper, 1986; Dixon et al., 1997). The highest reported CO_2 concentration of all these studies is 1039 ppm from Cerro Negro, Nicaragua (Roggensack et al., 1997). In light of these studies, the CO_2 contents of MI from all compositions from Mount Erebus prove to be unusual.

The trend in CO_2 concentrations is similar to that of water, with few exceptions. Besides the DVDP basanites, only sample 97009 and an inclusion from samples 97011 and 97006 each contain appreciable CO_2. Again, this suggests that the magma sampled by the melt inclusions was trapped in a shallow, low pressure environment. If the magmas were related by fractional crystallization occurring at progressively shallower depths in the crust, the saturation pressures would be expected to decrease with magma evolution. This would probably be manifested as a more gradual decreasing trend on Figure 8. Such a trend would be of decreasing CO_2 solubility with fractional crystallization due to pressure and compositional effects (Figure 13).

The CO_2 solubility curves for samples AW82033 and 7713 support the interpretation, based on H_2O contents of MI, that the inclusions were trapped at low-pressure conditions. Their MI CO_2 contents are consistent with saturation pressure around 1 kbar assuming CO_2 is the only volatile phase present. The water solubility curves (Figure 12) indicate saturation pressures on the order of tens of bars, while the CO_2 solubility curves (Figure 13) indicate saturation pressures on the order of 1 kbar. The saturation pressure considering both volatiles is probably slightly higher than the CO_2 solubility estimate given the shape of the CO_2/H_2O saturation isobars (Figure 14). This illustrates the importance of considering both volatiles when determining saturation pressures.

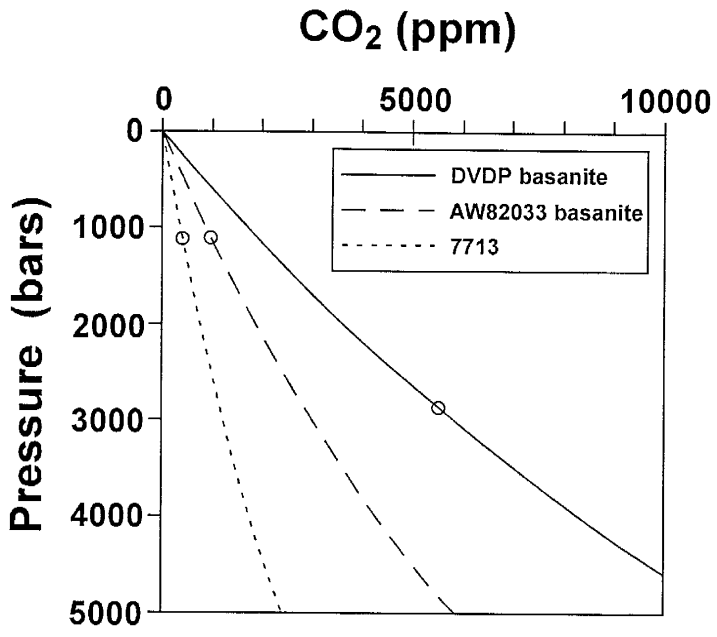

Figure 13. Carbon dioxide solubility curves modeled for DVDP basanite (solid line), AW82033 basanite melt inclusions (dashed line), and sample 7713 (dotted line) at 1200°C. Circles indicate the mean melt inclusion composition for each sample at its corresponding saturation pressure. The solubility curves are based on extrapolations of the compositional effects of alkali basalts on CO_2 solubility, thus have potentially large errors for the more evolved melt compositions. Solubilities modeled after Dixon (1997).

Figure 14 is a vapor saturation diagram modeled for the DVDP basanite composition at 1200°C. The diagram was constructed using the CO_2 solubility model of Dixon (1997) and the H_2O solubility model of Dixon et al. (1995). One of the compositions used in the calibration of their CO_2 solubility model is the leucitite of Thibault and Holloway (1994) which is chemically very similar to the basanite of this study. CO_2 fugacities were determined using the modified Redlich-Kwong equation of state and Gibbs free energies of Bottinga and Richet (1981). The water speciation model of Dixon et al. (1995) was also used. The model assumes Henrian mixing between H_2O and CO_2 in the melt.

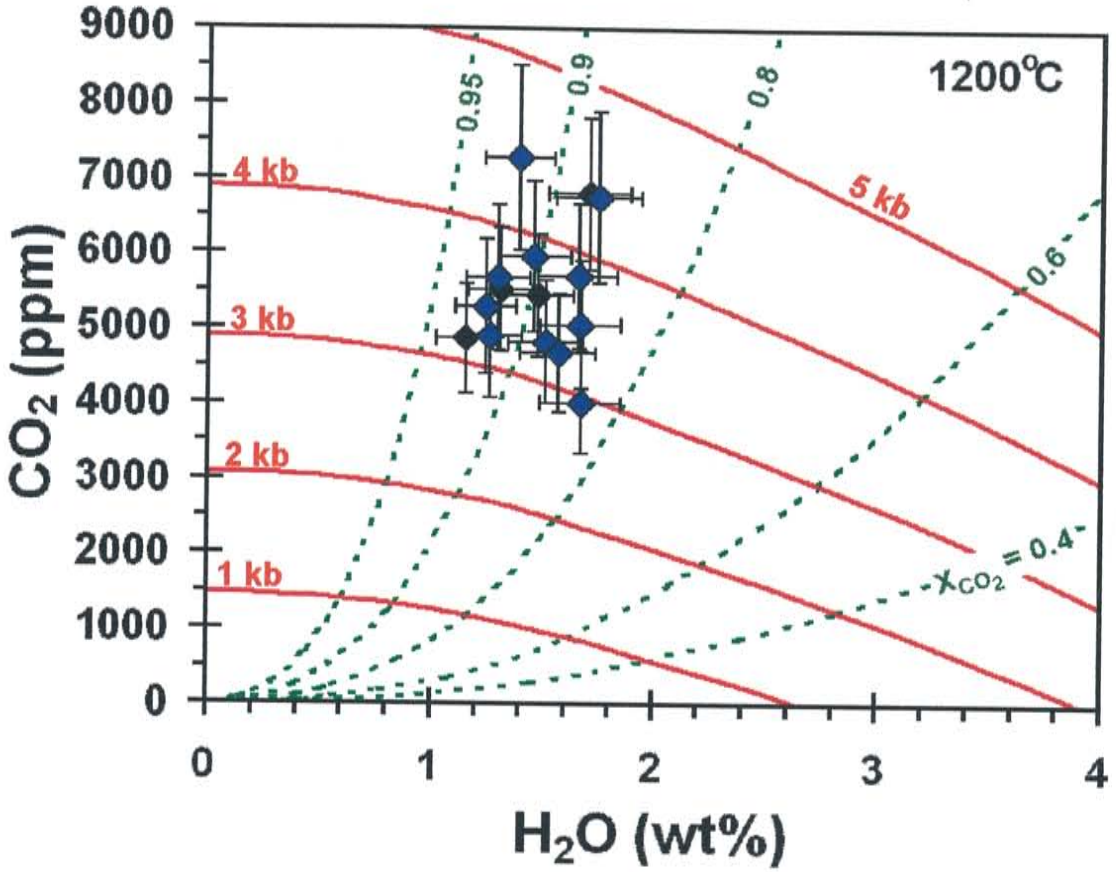

Figure 14. Vapor saturation diagram modeled for basanite at 1200°C. Solid contours represent the isobaric range of melt compositions in equilibrium with an H_2O-CO_2 vapor. Intersection of the isobar (red contours) with the X-axis is equal to the end-member solubility of H_2O, and intersection of the isobar with the Y-axis equals the CO_2 solubility. Dashed (green) contours are isopleths for the composition of exsolved fluid in equilibrium with the silicate melt. Interpolation of the MI compositions yields the minimum pressure at which the inclusion could have been trapped, and the composition of fluid exsolved from the melt at that pressure. Error bars represent 2σ uncertainty of the basanite melt inclusion H_2O and CO_2 analyses.

It is important to use a two component saturation diagram such as Figure 14, because calculating the saturation pressure based on a single volatile component in a system that contains significant amounts of more than one volatile component will grossly underestimate the saturation pressure. The diagram gives the pressure at which the magma must have begun degassing. The saturation pressure also provides a minimum

pressure of melt inclusion entrapment. On this diagram, the solid contours are saturation isobars, which indicate the pressure of saturation. The dashed contours are saturation isopleths, which give the composition of the degassing vapor in terms of mole fraction CO_2 in the vapor (Dixon, 1997). The basanite melt inclusion data plotted on this diagram indicate saturation pressures of 3-4.5 kbar. These saturation pressures indicate that the MI were trapped at minimum depths of 9 to 13 km. At these pressures and compositions, the exsolved vapor phase is about 90% mole fraction CO_2.

Implications to Degassing

Excess volatiles have been noted for numerous volcanoes with varying eruptive styles (Andres et al., 1991; Westrich and Gerlach, 1992; Gerlach and McGee, 1994; Allard et al., 1994; Kazahaya, et al., 1994; Allard, 1997). As volcanic gas studies progress, excess volatile degassing appears to be the rule rather than the exception. Sources invoked to produce these volatiles include: unerupted magma in the subvolcanic reservoir, a separate vapor phase present in the magma (vapor accumulation), and decomposition of volatile bearing mineral phases (anhydrite) (Wallace and Gerlach, 1994). Vapor accumulation and mineral decomposition can safely be ruled out for Mount Erebus because the open system (convecting lava lake) would not permit vapor trapping, and there is no evidence for carbonate or sulfate minerals in any of the lavas. The most realistic explanation is unerupted magma. Many questions remain to be answered regarding this magma. Where is the magma responsible for the volatiles? What is the composition of this magma? How is this magma degassing?

In order to answer some of these questions degassing has been modeled using the volatile concentrations of basanite melt inclusions. The volatile flux can be estimated

using volatile concentrations of melt inclusions compared to those of matrix glass of ejecta and scaled to magma flux or volume magma erupted (Devine et al., 1984). First, the magma flux must be determined. This is difficult to determine for Mount Erebus, because of the extensive recycling of the magma in the lava lake. The convection rate of the lake does not represent the flux of fresh, undegassed magma. Harris et al. (in press) used thermal emissions of the lava lake measured by satellite to determine the heat lost from the lake. This heat loss was converted to magma solidified (the amount of magma cooled in order to produce observed heat). They calculated fluxes of solidifying magma of the Mount Erebus lava lake of 3500-4300 Mg/day for 1985, and 1500-2300 Mg/day for 1989. Esser (1996) determined a long term erupted magma flux using $^{40}Ar/^{39}Ar$ ages of lavas and volume estimates. His estimate for the eruption rate of lava for the whole of Mount Erebus is 1.7 km^3/ky (~12,000 Mg/day).

Table 4 shows the observed volatile fluxes of Mount Erebus compared with theoretical fluxes. The magma flux range of Harris et al. (in press) was used to determine theoretical fluxes. For the sake of argument, these fluxes are assumed to roughly equal the flux of fresh phonolite magma entering the system. The gas fluxes were determined by scaling the concentration of volatiles in basanite melt inclusions to 75% fractional crystallization to phonolite and subtracting the concentration of volatiles in the matrix glass of sample 97018. This value is the effective concentration of the volatiles lost to degassing from the fractionation of the basanite to phonolite and the accompanying rise to the surface. This mass fraction was multiplied by the mass flux of fresh magma (phonolite) entering the system. The volatiles are assumed perfect incompatible elements.

This gives a petrologic estimate of the gas flux given fractional crystallization from basanite to phonolite.

Table 3. Petrologic Degassing Estimate

Species	Observed Flux (Mg/day)	Theoretical Flux (Mg/day)					
Magma		1500	1500 Corr.[c]	4000	4000 Corr.[c]	4300	4300 Corr.[c]
SO_2	21-71[a]	25		67		72	
HCl	15-48[a]	3.2	3.0	8.6	8.0	9.3	8.6
HF	6-25[a]	7.0	0.9	18.5	2.3	20	2.5
H_2O		89		236		254	
CO_2	≈2000[b]	44[d]		116[d]		125[d]	
		33[e]		88[e]		95[e]	

[a] Zreda-Gostynska et al., 1997. [b] L.J. Wardell, pers. comm. [c] HCl, HF fluxes corrected for 8.2 wt% apatite crystallization of basanite (see text). [d] CO_2 flux based on highest basanite [CO_2] = 7270. [e] CO_2 flux based on mean basanite [CO_2] = 5520

The assumption that fluorine and chlorine are perfectly incompatible elements is not valid because both elements are partitioned into apatite. Therefore, corrected gas fluxes were determined for these species by removing the F and Cl involved with crystallizing 8.2 wt% apatite from the parental basanite. This is the amount of apatite fractionation required to reconcile the P_2O_5 contents of the glasses. The composition of apatite for this calculation was the average apatite found in the melt inclusions (Table D.5., Appendix D). The large fractionation of fluorine may by due to overestimated fluorine contents of the apatite crystals, as the electron microprobe analyses of the apatite standard yield F values above the accepted value (Appendix G). Sulfur also is not a perfect incompatible element as it partitions into Fe-sulfide. The amount of this phase that remains in the lava is small and assumed to be negligible.

The theoretical gas fluxes are reasonable approximations of the observed fluxes for all components except CO_2. The calculated fluxes are comparable for SO_2 and a

factor of 2-3 less for HF and HCl. Despite the high concentration of CO_2 in the basanite melt inclusions, the calculated CO_2 flux is an order of magnitude lower than the observed. This simplistic approach to degassing indicates volatiles are simultaneously undergoing open-system degassing from magma all through the fractional crystallization sequence.

The degassing model outlined above is certainly not the only rational scenario that can be envisioned. The magmatic flux could be significantly different from the model. However, it is difficult to reconcile the large amount CO_2 emitted relative to the other volatiles. If the magmatic flux was increased to account for the emitted CO_2, there would be a large quantity of S, F, and Cl that are not observed.

Kazahaya et al., (1994) have shown that effective degassing of excess volatiles can occur through magma convection in a conduit. The many observations of magma convection strongly suggest that this process occurs at Mount Erebus. However, assuming the contribution of fresh, undegassed phonolite is on the order of 4000 Mg/day, the degassing of the phonolite would contribute a scant fraction of the observed gas flux. If the phonolite was producing the gas, it would have to contain ~50 wt.% CO_2! The flux of phonolite would have to be unreasonably large to account for the gas emanating from the volcano. The system requires open system degassing from the parental basanite source. Even then, the basanite would have to contain over ten times the amount of CO_2 measured in the MI to account for the observed flux.

The likely source of the excess CO_2 is from basanite deeper in the system than the melt inclusions are recording (~4.5 kbar), possibly as deep as the partial melt zone in the

mantle. This suggests that there is a separate CO_2-rich fluid phase rising from depths greater than 13 km.

The derivation of excess CO_2 from the mantle is consistent with the wealth of information suggesting a close petrologic connection between CO_2 and highly alkaline, silica-undersaturated magmas. Many experimental studies have concluded that CO_2 as well as H_2O has a strong effect on the composition of the partial melt derived from peridotite mantle (Eggler, 1978; Wyllie, 1979; Edgar, 1987). These studies have shown that melting peridotite in the presence of CO_2 (as carbonate) produces alkaline, silica understaurated melts. A larger proportion of H_2O causes melting of a less alkaline and silica undersaturated melt (Eggler, 1978). These partial melts can be produced and maintained over a large range in temperature and have very high CO_2 solubilities (Wyllie and Huang, 1976). The experimental studies show that a carbonated mantle is required to produce a basanite melt. This melt can contain large amounts of CO_2 at the temperatures and pressures of formation but will degas much of the CO_2 as it rises and solubility drops dramatically (Wyllie and Huang, 1976; Wyllie, 1979). As the CO_2-rich fluid rises and decompresses it is heated due to the Joule-Thompson Effect (Spera, 1984). This heating of the fluid will help to maintain the temperature of the magma throughout the system. Derivation of the CO_2 in the Mount Erebus gas plume is consistent with experimental evidence of alkaline magma production and solubilities of these magmas at their origin.

CONCLUSIONS

The series of lavas at Mount Erebus provide a remarkably complete fractional crystallization sequence from basanite to phonolite compositions. The chemistry of melt inclusions trapped in phenocrysts from these lavas record the process of this magma evolution. Major and trace element compositions of the melt inclusions support the model that these lavas are related by simple fractional crystallization of the observed crystal assemblage (Kyle et al., 1992).

Volatile concentrations in the melt inclusions suggest that magma evolution is accompanied by continuous degassing. H_2O and CO_2 degas with magma fractionation due largely to the decrease in pressure as the more evolved magmas are emplaced progressively higher in the crust. Pre-eruptive sulfur contents gradually decrease, indicating sulfur continuously degasses with magma evolution. The water-bearing fluid phase, thought to be produced during magmatic evolution and ascent, scavenges fluorine and chlorine from the magma. Volatile concentrations in melt inclusions provide strong evidence that open system degassing occurs from basanite to phonolite at Mount Erebus.

The volatile contents of MI also provide information about crystallization depths and therefore magma chamber depths. The water contents of the more evolved lava compositions are consistent with saturation on the order of tens of bars. However, when the CO_2 contents are considered, the saturation pressure is on the order of 1 kbar. These saturation pressures indicate that the magmas resided and crystallized at relatively shallow depths (<5 km).

Comparison of volatile contents in melt inclusions with current magmatic fluxes suggest much of the gas plume is derived from deep within the magma system. Volatile

concentrations of basanite melt inclusions indicate the magma degasses a CO_2-rich fluid at depths of at least 13 km. However, the amount of CO_2 that can be attributed to this degassing does not account for the large CO_2 flux emanating from the volcano. Additional CO_2 from deeper in the system, perhaps as deep as the mantle is required to explain the gas flux. A CO_2-rich fluid is therefore migrating from depths greater than 13 km to the surface under open system conditions.

REFERENCES

Allard, P., 1997. Endogenous magma degassing and storage at Mount Etna. *Geophysical Research Letters* **24,** 2219-2222.

Allard, P., Carbonnelle, J., Metrich, N., Loyer, H., Zettwoog, P., 1994. Sulfur output and magma degassing budget of Stromboli volcano. *Nature* **368,** 326-330.

Anderson, A.T., 1974. Chlorine, sulfur, and water in magmas and oceans. *Geological Society of America Bulletin* **85,** 1485-1492.

Anderson, A.T., Brown, G.G., 1993. CO_2 contents and formation pressures of some Kilauean melt inclusions. *American Mineralogist* **78,** 794-803.

Andres, R.J., Rose, W.I., Kyle, P.R., deSilva, S., Francis, P., Gardeweg, M., Moreno Roa, H., 1991. Excessive sulfur dioxide emissions from Chilean volcanoes. *Journal of Volcanology and Geothermal Research* **46,** 323-329.

Blank, J.G., Brooker, R.A., 1994. Experimental studies of carbon dioxide in silicate melts: solubility, speciation, and stable carbon isotope behavior. In: Carroll, M.R., Holloway, J.R., (eds.) *Volatiles in Magmas, Mineralogical Society of America, Reviews in Mineralogy* **30,** 157-186.

Bottinga, Y., Richet, P., 1981. High pressure and temperature equation of state and calculation of the thermodynamic properties of carbon dioxide. *American Journal of Science* **281,** 615-660.

Carroll, M.R., Blank, J.G., 1997. The solubility of H_2O in phonolite melts. *American Mineralogist* **82,** 549-556.

Carroll, M.R., Webster, J.D., 1994. Solubilities of sulfur, noble gases, nitrogen, chlorine, and fluorine in magmas. In: Carroll, M.R., Holloway, J.R., (eds.) *Volatiles in Magmas, Mineralogical Society of America, Reviews in Mineralogy* **30,** 231-279.

Cawthorn, R.G., Collerson, K.D., 1974. The recalculation of pyroxene end-member parameters and the estimation of ferrous and ferric iron content from electron microprobe analyses. *American Mineralogist* **59,** 1203-1208.

Devine, J.D., Sigurdsson, H., Davis, A.N., Self, S., 1984. Estimates of sulfur and chlorine yield to the atmosphere from volcanic eruptions and potential climatic effects. *Journal of Geophysical Research* **89,** 6309-6325.

Dixon, J.E., Pan, V., 1995. Determination of the molar absorptivity of dissolved carbonate in basanitic glass. *American Mineralogist* **80,** 1339-1342.

Dixon, J.E., Stolper, E.M., Holloway, J.R., 1995. An experimental study of water and carbon dioxide solubilities in mid-ocean ridge basaltic liquids. Part I: Calibration and solubility models. *Journal of Petrology* **36,** 1607-1631.

Dixon, J.E., Stolper, E.M., 1995. An experimental study of water and carbon dioxide solubilities in mid-ocean ridge basaltic liquids. Part II: Applications to degassing. *Journal of Petrology* **36,** 1633-1646.

Dixon, J.E., 1997. Degassing of alkalic basalts. *American Mineralogist* **82,** 368-378.

Dixon, J.E., Clague, D.A., Wallace, P., Poreda, R., 1997. Volatiles in alkalic basalts from the North Arch Volcanic Field, Hawaii: Extensive degassing of deep submarine-erupted alkalic series lavas. *Journal of Petrology* **38,** 911-939.

Dunbar, N.W., Cashman, K.V., Dupré, R., 1994. Crystallization processes of anorthoclase phenocrysts in the Mount Erebus magmatic system: Evidence from crystal composition, crystal size distributions, and volatile contents of melt inclusions. *Volcanological and Environmental Studies of Mount Erebus, Antarctica, Antarctic Research Series* **66,** 129-146.

Edgar, A.D., 1987. The genesis of alkaline magmas with emphasis on their source regions: inferences from experimental studies. In: Fitton, J.G., Upton, B.G.J. (eds.) *Alkaline Igneous Rocks.* Geological Society Special Publication No. 30., pp. 29-52.

Eggler, D.H., 1978. The effect of CO_2 upon partial melting of peridotite in the system Na_2O-CaO-Al_2O_3-MgO-SiO_2-CO_2 to 35 kb, with an analysis of melting in a peridotite-H_2O-CO_2 system. *American Journal of Science* **278,** 305-343.

Esser, R.P., 1996. $^{40}Ar/^{39}Ar$ Dating of Mount Erebus Volcano, Antarctica. M.S. Thesis, New Mexico Institute of Mining and Technology, Socorro, New Mexico.

Fine, G., Stolper, E., 1986. Dissolved carbon dioxide in basaltic glasses: concentrations and speciation. *Earth and Planetary Science Letters* **76,** 263-278.

Gerlach, T.M., McGee, K.A., 1994. Total sulfur dioxide emissions and pre-eruption vapor-saturated magma at Mount St. Helens, 1980-88. *Geophysical Research Letters* **21,** 2833-2836.

Harris, A.J.L., Flynn, L.P., Rothery, D.A., Oppenheimer, C., (In press) Lava lakes from space. *Journal of Geophysical Research*

Ihinger, P.D., Hervig, R.L., McMillan, P.F., 1994. Analytical methods for volatiles in glasses. In: Carroll, M.R., Holloway, J.R., (eds.) *Volatiles in Magmas, Mineralogical Society of America, Reviews in Mineralogy* **30,** 67-121.

Jarosewich, E., Nelen, J.A., Norberg, J.A., 1980. Reference samples for electron microprobe analysis. *Geostandards Newsletter* **4,** 43-47.

Johnson, M.C., Anderson, A.T., Rutherford, M.J., 1994. Pre-eruptive volatile contents of magmas. In: Carroll, M.R., Holloway, J.R., (eds.) *Volatiles in Magmas, Mineralogical Society of America, Reviews in Mineralogy* **30,** 281-330.

Kazahaya, K., Shinohara, H., Saito, G., 1994. Excessive degassing of Izu-Oshima volcano: magma degassing in a conduit. *Bulletin Volcanology* **56,** 207-216.

Kyle, P.R., 1977. Mineralogy and glass chemistry of recent volcanic ejecta from Mount Erebus, Ross Island, Antarctica. *New Zealand Journal of Geology and Geophysics* **20,** 1123-1146.

Kyle, P.R., Treves, S.B., 1974. Geology of DVDP 3, Hut Point Peninsula, Ross Island, Antarctica. Preliminary Site Report. Dry Valley Drilling Project. Northern Illinois University, Bulletin No. 3, 13-48.

Kyle, P.R., Dibble, R.R., Giggenbach, W.F., Keys, J., 1982. Volcanic activity associated with the anorthoclse phonolite lava lake, Mount Erebus, Antarctica. In *Antarctic Geosciences,* 1st ed., vol. **1**, ed. C Craddock, University of Wisconsin Press, 735-745.

Kyle, P.R., Meeker, K., Finnegan, D., 1990. Emission rates of sulfur dioxide, trace gases and metals from Mount Erebus, Antarctica. *Geophysical Research Letters* **17,** 2125-2128.

Kyle, P.R., Moore, J.A., Thirlwall, M.F., 1992. Petrologic evolution of anorthoclase phonolite lavas at Mount Erebus,Ross Island, Antarctica. *Journal of Petrology* **33,** 849-875.

Lange, R.A., Carmichael, I.S.E., 1987. Densities of Na2O-K2O-CaO-MgO-FeO-Fe2O3-Al2O3-TiO2-SiO2 liquids: New measurements and derived partial molar properties. *Geochimicaet Cosmochimica Acta* **51,** 2931-2946.

LeBas, M.J., Le Maitre, R.W., Streckeisen, A., Zanettin, B., 1986. A chemical classification of volcanic rocks based on the total alkali-silica diagram. *Journal of Petrology* **27,** 745-750.

Lowenstern, J.B., 1995. Applications of silicate-melt inclusions to the study of magmatic volatiles. In: Thompson, J.F.H. (ed.) *Magmas, Fluids, and Ore Deposits, Mineralogical Association of Canada Short Course Series* **23,** 71-99.

Metrich, N., Clocchiatti, R., 1989. Melt inclusion investigation of the volatile behaviour in historic alkali basaltic magmas of Etna. *Bulletin Volcanology* **51,** 185-198.

Metrich, N., Sigurdsson, H., Meyer, P.S., Devine, D., 1991. The 1783 Lakigagar eruption in Iceland: geochemistry, CO_2 and sulfur degassing. *Contributions to Mineralogy and Petrology* **107,** 435-447.

Moore, G., Vennemann, T., Carmichael, I.S.E., 1998. An empirical model for the solubility of H_2O in magmas to 3 kilobars. *American Mineralogist* **83,** 36-42.

Moore, J.A., Kyle, P.R., 1987. Volcanic geology of Mount Erebus, Ross Island, Antarctica. *Proceedings of the NIPR Symposium on Antarctic Geosciences.* **1,** 48-65.

Morimoto, N., 1989. Nomenclature of pyroxenes. *Canadian Mineralogist* **27,** 143-156.

Poulson, S.R., Ohmoto, H., 1990. An evaluation of the solubility of sulfide sulfur in silicate melts from experimental data and natural samples. *Chemical Geology* **85,** 57-75.

Roggensack, K., Hervig, R.L., McKnight, S.B., Williams, S.N., 1997. Explosive basaltic volcanism from Cerro Negro volcano: Influence of volatiles on eruptive style. *Science* **277,** 1639-1642.

Spera, F.J., 1984. Carbon dioxide in petrogenesis III: role of volatiles in the ascent of alkaline magma with special reference to xenolith-bearing mafic lavas. *Contributions to Mineralogy and Petrology* **88,** 217-232.

Stolper, E., 1982. Water in silicate glasses: An infrared spectroscopic study. *Contributions to Mineralogy and Petrology* **81,** 1-17.

Thibault, Y., Holloway, J.R., 1994. Solubility of CO_2 in a Ca-rich leucitite: effects of pressure, temperature, and oxygen fugacity. *Contributions to Mineralogy and Petrology* **116,** 216-224.

Wallace, P.J, Anderson, A.T., 1998. Effects of eruption and lava drainback on the H_2O contents of basaltic magmas at Kilauea Volcano. *Bulletin Volcanology* **59,** 327-344.

Wallace, P.J, Carmichael, I.S.E, 1992. Sulfur in basaltic magmas. *Geochimica et Cosmochimica Acta* **56,** 1863-1874.

Wallace, P.J, Gerlach, T.M., 1994. Magmatic vapor source for sulfur dioxide released during volcanic eruptions: Evidence from Mount Pinatubo. *Science* **265,** 497-499.

Webster, J.D., Kinzler, R.J., Mathez, E.A., (In press) Chloride and water solubility in basalt and andesite liquids and implications for magmatic degassing. *Geochimica et Cosmochimica Acta*

Wendtlandt, R.F., 1982. Sulfide saturation of basalt and andesite melts at high pressures and temperatures. *American Mineralogist* **67,** 877-885.

Westrich, H.R., Gerlach, T.M., 1992. Magmatic gas source for the stratospheric SO_2 cloud from the June 15, 1991, eruption of Mount Pinatubo. *Geology* **20,** 867-870.

Wyllie, P.J., 1979. Magmas and volatile components. *American Mineralogist* **64,** 469-500.

Wyllie, P.J., Huang, W.L., 1976. High CO_2 solubilities in mantle magmas. *Geology* **4,** 21-24.

Zreda-Gostynska, G., Kyle, P.R., Finnegan, D., Prestbo, K.M., 1997. Volcanic gas emissions from Mount Erebus and their impact on the Antarctic environment. *Journal of Geophysical Research* **102,** 15,039-15,055.

Appendix A. Sample Localities and Rock Descriptions

The samples were selected based on the degree of quenching. Rapid quenching is critical for melt inclusion studies to avoid post-entrapment alteration of the inclusions. For this reason, hyaloclastites, pillow breccias, and bombs were selected for study. Pillow lava and dike rinds were also collected but were insufficiently quenched and were eliminated from the study.

DVDP 3-283 and DVDP 3-295 are drill core samples from the Dry Valley Drilling Project on Hut Point Peninsula (Kyle and Treves, 1974). These samples are from the third drill core taken on Hut Point from depths of 283 and 295 meters. Both samples are black, olivine and pyroxene phyric, basanite pillow breccias.

7713, AW82033, and 97006 are from Turks Head. Samples 7713 and AW82033 are sand and gravel sized plagioclase-phyric, palagonite breccias. 7713 is a lava lobe sample that is partially brecciated (gradational between lava and palagonite breccia). AW82033 is mostly disintegrated with few angular glassy lava bits throughout. Sample 97006 is a glassy, anorthoclase bearing lava flow top located on the top of the Turks Head exposure.

97009 is a tephriphonolite palagonite breccia sample from the south-eastern portion of Inaccessible Island. The deposit is mostly yellow, sand-sized, bedded palagonite breccia with rare scoriacious lapilli clasts scatted throughout the unit.

97010 and 97011 are black, plagioclase (minor) phyric, pillow lava breccias from Tent Island. 97010 was collected from the south-eastern portion of the island while 97011 was collected from the south-western portion of the island. Both samples appear similar. 97011 is perhaps higher in the stratigraphy than is 97010.

97018 and EA1 are from the summit of Mount Erebus. 97018 is a bomb that erupted from the lava lake on December 21, 1997. EA1 is a single anorthoclase crystal from the crater rim and is of unknown age, but is almost certainly less than 100 years old.

Table A.1. Sample Locations and Rock Type

Sample	Location	Composition*	Occurance
DVDP 3-283	Hut Point	Basanite	Drill core/hyaloclastite
DVDP 3-283	Hut Point	Basanite	Drill core/ hyaloclastite
AW82033	Turks Head	Basanite	Palagonite breccia
7713	Turks Head	Phonotephrite	Palagonite breccia
97006	Turks Head	Tephriphonolite	Lava flow top
97009	Inaccessible Is.	Tephriphonolite	Palagonite breccia
97010	Tent Island	Tephriphonolite	Pillow breccia
97011	Tent Island	Phonotephrite	Pillow breccia
97018	Mt. Erebus Summit	Phonolite	Bomb
EA1	Mt. Erebus Summit	Phonolite	Single Anorthoclase crystal

* Compositions based on whole rock analyses.

Appendix B: FTIR Sample Preparation and Quantification

FTIR Sample Preparation

Crystals were separated from the crushed samples by magnetic separation and heavy liquids. Crystals with melt inclusions were hand picked under mineral oil using a binocular microscope. The grains were mounted following the procedure of Newman et al. (1986). This procedure involves mounting the grains in Orthodontic Resin (L.D. Caulk Co.) on glass. A crystal is placed in the center of a 1" round frosted glass slide. The powder polymer resin is spread evenly over the slide so that the grain is covered. The powder is then saturated with the liquid portion of the resin mixture using a glass, medicine dropper. Doubly polished wafers were prepared by grinding the grains on a machine lap (320 and 600 grit) followed by hand polishing with loose diamond grit (15, 6, 1 μm). The machine laps were used to polish through the grain until just short of intersecting the inclusion. The inclusions were then intersected and brought to high polish using the loose diamond on Texmet (Buehler Co.) polishing cloths using deionized water as a lubricant. The grains (and their mounts) were lifted from the slide with a pen knife after soaking the slides in water for several hours. The grain mount was then trimmed using a scissors to roughly 1 cm square. The opposite side of the inclusion was polished by reattaching the mount to the slide on the opposite side with super-glue (applied around perimeter of mount). The polishing procedure was repeated such that each side of the inclusion was polished, and at least a 20×20 μm area through the inclusion was free of obstructions.

Data Collection

Transmission spectra of the glasses were obtained for the wave number range of 600-6000 cm^{-1} on a Nicolet Magna-IR 750 spectrometer with a Spectra Tech infrared microscope attachment. For each spectrum, the infrared beam was aimed optically by focussing onto the surface of the inclusion using the infrared lens. The outgoing beam was focussed into the detector by adjusting the condenser until the bottom aperture came into focus. The lower aperture (between sample and detector) was adjusted in size and position to the desired area. The upper aperture (between source and sample) was adjusted to duplicate to configuration of the lower aperture. Bubbles and crystals in the inclusions were avoided by appropriate selection of the aperture configuration. The spectra were recorded as absorbance versus wavenumber charts and hard copies were made. The background was separated from the peaks by hand drawing the background using a french curve. A minimum estimate and a reasonable yet conservative background line was drawn. The difference between the two backgrounds was taken to be the error estimate below the true value. This error was used for both the plus and minus error estimate. The peak height was then measured using a Gerber Variable-scale.

The concentration of the dissolved water and carbonate were quantified using the Beer-Lambert Law (Stolper, 1982; Fine and Stolper, 1986):

$$C = \frac{MW \times Abs}{d \times \rho \times \varepsilon}$$

Where C is the concentration of H_2O or CO_3^{-2} expressed as a weight fraction, MW is the molecular weight of H_2O or CO_2, Abs is the height of the absorption peak, d is the thickness in centimeters, ε is the molar absorptivity (extinction coefficient) in liters/mol cm, and ρ is the density of the glass in g/liter. The thickness of the wafer was

measured using a Mitutoyo digital displacement micrometer which has an uncertainty of 1-2 μm. The density of the glass was calculated on a dry basis using the method of Lange and Carmichael (1987).

The fundamental OH-stretching peak at ~3550 cm^{-1} was used to determine the total water concentration of the glasses (Stolper, 1982). The molar absorptivity for basalt of the 3550 cm^{-1} peak is 63±5 (Dixon et al., 1988). This value was used for basanite and phonotephrite compositions. The molar absorptivity for the water peak in phonolite samples was determined to be 82.6±6.5 (2σ) from a 1 wt% H_2O experimental phonolite sample of Carroll and Blank (1997). Carbonate was determined using the doublet peaks near 1610 and 1375 cm^{-1}. The molar absorptivity of these peaks are assumed to be the same and were determined using the empirical equation of Dixon and Pan (1995). Their equation $\varepsilon = 451\text{-}342\times(Na/(Na+Ca))$ relates the molar absorptivity of carbonate to the molar Na and Ca content of the glass. The measured quantities (thickness, absorbance peak heights) are listed in Table B.1. The calculated densities and extinction coefficients are listed in Table B.2.

Table B.1. FTIR Thickness and Peak Height Measurements

Inclusion	Thickness (cm)	3550 cm^{-1}	1610 cm^{-1}	1375 cm^{-1}	Host
283a	0.0053	0.661 (0.006)	0.627 (0.020)	0.604 (0.023)	Ol
283a#2	0.0053	0.661 (0.005)	0.621 (0.017)	0.598 (0.017)	Ol
283b	0.0062	0.662 (0.006)	0.627 (0.017)	0.595 (0.020)	Ol
283b#2	0.0062	0.680 (0.003)	0.654 (0.020)	0.616 (0.020)	Ol
283c	0.0063	0.883 (0.011)	0.741 (0.015)	0.703 (0.014)	Ol
283d	0.0068	0.843 (0.003)	0.593 (0.024)	0.558 (0.021)	Ol
283f	0.0052	0.732 (0.003)	0.668 (0.021)	0.644 (0.022)	Ol
283h	0.0068	1.105 (0.007)	0.993 (0.019)	0.954 (0.026)	Ol
295a	0.0041	0.647 (0.004)	0.485 (0.007)	0.464 (0.007)	Ol
295b	0.0059	0.939 (0.007)	0.494 (0.012)	0.468 (0.011)	Ol
295c	0.0045	0.626 (0.006)	0.561 (0.011)	0.530 (0.008)	Ol
295d	0.0047	0.748 (0.009)	0.491 (0.008)	0.474 (0.015)	Ol
295e	0.0057	0.820 (0.007)	0.570 (0.022)	0.548 (0.026)	Ol
295f	0.0088	1.075 (0.011)	0.443 (0.018)	0.430 (0.023)	Ol
295g	0.0067	1.119 (0.007)	0.936 (0.018)	0.906 (0.018)	Ol
295h	0.0085	1.127 (0.012)	0.178 (0.019)	0.178 (0.032)	Ol
295l	0.0056	0.693 (0.002)	0.656 (0.019)	0.637 (0.019)	Ol
295j	0.0067	0.806 (0.005)	0.685 (0.014)	0.650 (0.018)	Ol
295k	0.0063	0.941 (0.009)	0.348 (0.019)	0.334 (0.023)	Ol
295l	0.0060	0.897 (0.005)	0.579 (0.018)	0.561 (0.021)	Ol
295m	0.0057	0.788 (0.005)	0.282 (0.016)	0.266 (0.013)	Ol
295n	0.0050	0.772 (0.002)	0.291 (0.013)	0.278 (0.013)	Ol
295o	0.0074	0.346 (0.002)	0.104 (0.007)	0.090 (0.007)	Ol
295p	0.0071	0.379 (0.003)	0.409 (0.014)	0.398 (0.013)	Ol
295q	0.0053	0.629 (0.004)	0.584 (0.015)	0.557 (0.015)	Ol
295r	0.0055	0.730 (0.002)	0.833 (0.018)	0.796 (0.018)	Ol
7713a1	0.0044	0.049 (0.005)	0.025 (0.008)	0.022 (0.008)	Plag
7713a2	0.0044	0.042 (0.004)	ND		Plag
7713b#1	0.0038	0.128 (0.003)	ND		Plag
7713b#2	0.0038	0.166 (0.005)	ND		Plag
7713c1	0.0106	0.720 (0.013)	0.055 (0.021)	0.061 (0.018)	Plag
7713c2	0.0106	0.603 (0.012)	ND		Plag
7713d	0.0036	0.280 (0.005)	0.026 (0.006)	0.028 (0.009)	Plag
7713e	0.0085	0.091 (0.002)	0.041 (0.011)	0.040 (0.013)	Ol
7713f	0.0065	0.058 (0.002)	0.040 (0.010)	0.038 (0.010)	Ol
7713g	0.0059	0.065 (0.003)	0.044 (0.009)	0.037 (0.015)	Ol
7713h	0.0054	0.052 (0.002)	0.036 (0.009)	0.027 (0.006)	Ol
7713l	0.0052	0.041 (0.003)	0.035 (0.006)	0.026 (0.006)	Ol
7713j	0.0077	0.080 (0.005)	0.055 (0.010)	0.055 (0.011)	Ol
7713k	0.0051	0.063 (0.003)	0.054 (0.010)	0.052 (0.015)	Ol
7713l	0.0056	0.040 (0.005)	0.019 (0.005)	0.017 (0.006)	Ol
7713-1	0.0077	0.066 (0.003)	ND		Ol

Table B.1. Continued

Inclusion	Thickness (cm)	3550 cm^{-1}	1610 cm^{-1}	1375 cm^{-1}	Host
97006a	0.0046	0.046 (0.002)	0.040 (0.008)	0.028 (0.011)	Ol
97006c	0.0077	0.072 (0.004)	0.118 (0.023)	0.106 (0.030)	Ol
97006d1	0.0074	0.057 (0.004)	0.065 (0.017)	0.06 (0.018)	Ol
97006d2	0.0074	0.070 (0.005)	0.076 (0.013)	0.068 (0.013)	Ol
97006-1	0.0099	0.128 (0.004)	0.031 (0.011)	0.023 (0.008)	Ol
97006-2	0.0068	0.073 (0.002)	ND		Ol
97006-3	0.0083	0.120 (0.006)	ND		Ol
97009a	0.0034	0.223 (0.003)	0.117 (0.007)	0.105 (0.01)	Ol
97009b	0.0072	0.470 (0.005)	0.141 (0.013)	0.140 (0.018)	Ol
97009c	0.0032	0.202 (0.004)	0.093 (0.006)	0.085 (0.012)	Ol
97009d	0.0052	0.262 (0.002)	0.085 (0.008)	0.077 (0.013)	Ol
97009e	0.0068	0.359 (0.005)	0.112 (0.013)	0.105 (0.016)	Ol
97009f	0.0031	0.108 (0.006)	0.082 (0.005)	0.070 (0.009)	Ol
97009g	0.0089	0.522 (0.006)	0.196 (0.024)	0.185 (0.017)	Ol
97009h	0.0044	0.219 (0.004)	0.151 (0.012)	0.134 (0.016)	Ol
97009I	0.0066	0.365 (0.006)	0.174 (0.009)	0.174 (0.015)	Ol
97009j	0.0031	0.227 (0.004)	0.120 (0.014)	0.113 (0.012)	Ol
97009-1	0.005	0.065 (0.002)	0.015 (0.005)	0.003 (0.002)	Ol
97009-2	0.0059	0.064 (0.002)	0.017 (0.010)	0.007 (0.003)	Ol
97009-3	0.0062	0.066 (0.002)	0.021 (0.008)	0.007 (0.005)	Ol
97010a	0.003	0.042 (0.003)	0.021 (0.005)	0.021 (0.006)	Ol
97010b	0.0041	0.055 (0.003)	0.084 (0.008)	0.075 (0.008)	Ol
97010c	0.005	0.059 (0.005)	0.028 (0.013)	0.023 (0.01)	Ol
97010d	0.0054	0.077 (0.004)	0.058 (0.007)	0.048 (0.009)	Ol
97010e	0.0032	0.047 (0.004)	ND		Ol
97010f	0.0041	0.059 (0.004)	0.030 (0.011)	0.030 (0.01)	Ol
97010g	0.0047	0.065 (0.002)	0.043 (0.013)	0.036 (0.014)	Ol
97010h	0.0044	0.053 (0.005)	0.023 (0.005)	0.017 (0.006)	Ol
97010I	0.0037	0.041 (0.003)	0.028 (0.006)	0.020 (0.008)	Ol
97011a1	0.004	0.051 (0.003)	0.049 (0.008)	0.049 (0.014)	Ol
97011a2	0.004	0.038 (0.003)	0.018 (0.006)	0.008 (0.003)	Ol
97011b	0.0045	0.054 (0.009)	0.029 (0.007)	0.027 (0.007)	Ol
97011c	0.0059	0.065 (0.006)	0.032 (0.007)	0.019 (0.010)	Ol
97011d	0.0031	0.028 (0.006)	0.032 (0.009)	0.029 (0.013)	Ol
97011e	0.0053	0.049 (0.004)	0.106 (0.023)	0.106 (0.021)	Ol
97011f	0.0031	0.041 (0.015)	0.032 (0.008)	0.030 (0.009)	Ol
97011g	0.0026	0.028 (0.003)	0.012 (0.004)	0.010 (0.004)	Ol
97018a	0.015	0.237 (0.005)	0.069 (0.031)	0.069 (0.031)	An
97018b	0.0144	0.245 (0.003)	0.080 (0.014)	0.063 (0.010)	An
97018c	0.0084	0.014 (0.002)	0.046 (0.018)	0.028 (0.016)	An
97018d	0.019	0.276 (0.004)	0.101 (0.037)	0.074 (0.028)	An
97018e	0.019	0.331 (0.003)	0.144 (0.055)	0.103 (0.048)	An
97018f	0.0094	0.136 (0.003)	0.042 (0.019)	0.038 (0.017)	An
97018g	0.0208	0.294 (0.003)	0.156 (0.055)	0.138 (0.073)	An
97018-1	0.0154	0.125 (0.003)	0.055 (0.030)	0.049 (0.018)	An
97018-2	0.0139	0.202 (0.003)	0.076 (0.023)	0.065 (0.030)	An

Table B.1. Continued

Inclusion	Thickness (cm)	3550 cm^{-1}	1610 cm^{-1}	1375 cm^{-1}	Host
AW82033a	0.0079	0.133 (0.001)	0.08 (0.009)	0.066 (0.007)	Ol
AW82033b	0.0091	0.208 (0.002)	0.045 (0.009)	0.046 (0.011)	Ol
AW82033c	0.0068	0.07 (0.003)	0.2 (0.03)	0.19 (0.02)	Ol
AW82033d	0.0054	0.056 (0.002)	0.116 (0.011)	0.116 (0.011)	Ol
AW82033e1	0.0074	0.028 (0.003)	0.22 (0.01)	0.216 (0.01)	Ol
AW82033e2	0.0074	0.129 (0.002)	0.249 (0.011)	0.249 (0.014)	Ol
AW82033f	0.0042	0.048 (0.003)	0.019 (0.006)	0.014 (0.005)	Ol
AW82033g	0.008	0.123 (0.002)	0.04 (0.014)	0.037 (0.014)	Ol
AW82033h	0.0134	0.428 (0.004)	0.393 (0.022)	0.0374 (0.031)	Ol
AW82033I	0.0064	0.068 (0.005)	0.152 (0.011)	0.143 (0.02)	Ol
AW82033j	0.0051	0.068 (0.004)	0.634 (0.014)	0.609 (0.015)	Ol
AW82033k	0.004	0.041 (0.003)	0.034 (0.004)	0.026 (0.007)	Ol
AW82033l	0.0038	0.038 (0.003)	0.029 (0.003)	0.0026 (0.006)	Ol
AW82033-1	0.0103	0.099 (0.003)	0.022 (0.01)	0.016 (0.008)	Ol
AW82033-2	0.103	0.096 (0.003)	0.025 (0.01)	0.01 (0.005)	Ol
AW82033-3	0.0135	0.124 (0.004)	0.02 (0.007)	0.009 (0.005)	Ol
EA1a	0.0177	0.304 (0.01)	0.107 (0.044)	0.073 (0.046)	An
EA1c	0.0158	0.3 (0.007)	0.091 (0.025)	0.091 (0.035)	An
EA1d	0.0124	0.213 (0.005)	0.07 (0.019)	0.067 (0.038)	An
EA1e	0.0208	0.407 (0.007)	0.064 (0.027)	0.079 (0.035)	An
EA1f	0.0097	0.214 (0.005)	0.049 (0.021)	0.049 (0.025)	An
EA1g	0.0285	0.472 (0.01)	0.167 (0.036)	0.174 (0.073)	An
EA1h	0.0127	0.249 (0.012)	0.083 (0.019)	0.07 (0.038)	An
EA1I	0.0243	0.414 (0.008)	0.142 (0.04)	0.16 (0.058)	An
EA1j	0.0195	0.306 (0.003)	0.135 (0.041)	0.138 (0.055)	An
EA1k	0.0206	0.421 (0.007)	0.102 (0.044)	0.087 (0.043)	An

Table B.2. Calculated Densities and Extinction Coefficients

Sample	Rock Type	Density (g/L)	ε_{H_2O} (L/mol×cm^2)	$\varepsilon_{CO_3^{2-}}$ (L/mol×cm^2)
DVDP 3-283	Basanite	2721 (180)	63 (5)	341 (22)
DVDP 3-295	Basanite	2725 (182)	63 (5)	329 (28)
7713	Phonotephrite	2593 (166)	63 (5)	237 (23)
97006	Phonolite	2443 (136)	82.6 (6.5)	155 (8)
97009	Tephriphonolite	2493 (154)	63 (5)	185 (16)
97010	Tephriphonolite	2474 (154)	63 (5)	177 (10)
97011	Phonolite	2446 (146)	63 (5)	168 (12)
97018	Phonolite	2428 (134)	82.6 (6.5)	145 (4)
AW82033	Basanite/PT	2662 (282)	63 (5)	287 (37)
EA1	Phonolite	2420 (132)	82.6 (6.5)	144 (7)

Numbers in parentheses represent 2σ uncertainties.

Table C.1. Melt Inclusion Compositions – Sample DVDP 3-283

Inclusion	a#1	b	c#1	h#2	Mean	StdDev
SiO_2	43.33	42.24	41.72	40.12	41.85	1.34
TiO_2	3.94	4.16	4.19	4.38	4.17	0.18
Al_2O_3	14.20	14.54	14.26	13.43	14.10	0.48
FeO_T	9.80	9.50	9.35	12.69	10.33	1.58
MnO	0.18	0.20	0.18	0.21	0.19	0.01
MgO	6.13	6.04	6.03	5.21	5.85	0.43
CaO	13.34	13.95	13.49	14.17	13.74	0.39
Na_2O	3.78	3.76	3.74	2.85	3.53	0.46
K_2O	1.60	1.61	1.62	1.33	1.54	0.14
P_2O_5	0.78	0.85	0.82	0.66	0.78	0.09
F (ppm)	2180	2030	1650	2050	1978	228
S (ppm)	1897	2167	2007	2072	2036	114
Cl (ppm)	710	850	820	580	740	122
Total*	97.55	97.34	95.83	95.51	96.56	1.04
H_2O (wt%)	1.31(0.14)	1.15(0.12)	1.47(0.16)	1.71(0.18)	1.41	0.24
CO_2 (ppm)	5510(820)	4860(710)	5440(770)	6790(960)	5648	815
CO_2/H_2O	0.42	0.42	0.37	0.40	0.40	N=4

Number in parentheses represents 2σ uncertainty of FTIR analysis.

Table C.1. Continued, Sample DVDP 3-295

Inclusion	a	b	c	d	g	i	j	l	q	r	Mean	StdDev
SiO_2	41.79	41.70	39.15	39.26	41.07	40.18	41.81	42.07	41.74	41.53	41.03	1.10
TiO_2	4.10	4.12	4.50	4.09	4.06	4.05	4.10	3.96	4.29	4.11	4.14	0.15
Al_2O_3	15.11	14.67	15.38	13.31	14.52	14.05	14.57	14.57	14.95	14.47	14.56	0.57
FeO_T	10.19	9.80	12.41	10.10	10.45	9.34	9.00	10.32	9.80	11.18	10.26	0.96
MnO	0.15	0.12	0.17	0.18	0.19	0.15	0.15	0.17	0.17	0.15	0.16	0.02
MgO	5.97	6.12	5.60	5.44	5.69	5.80	6.01	5.97	5.72	6.21	5.85	0.24
CaO	12.30	13.15	10.27	13.29	12.68	13.51	13.55	13.20	13.18	13.40	12.85	0.98
Na_2O	4.20	3.61	4.14	3.15	3.71	3.46	3.51	3.74	3.59	3.75	3.69	0.31
K_2O	1.80	1.62	1.90	1.50	1.47	1.53	1.58	1.59	1.60	1.69	1.63	0.13
P_2O_5	0.92	1.09	0.94	0.86	0.90	0.87	0.97	0.91	0.86	0.90	0.92	0.07
F (ppm)	1350	1380	1680	2030	1740	2060	1070	1260	1460	1690	1572	325
S (ppm)	2137	2062	2488	2267	2187	2352	2448	1787	1927	2007	2166	228
Cl (ppm)	670	890	870	1000	860	1020	610	1070	670	1090	875	175
Total	96.93	96.42	94.96	91.72	95.22	93.50	95.66	96.90	96.30	97.86	95.55	1.82
H_2O (wt%)	1.66(0.19)	1.67(0.18)	1.46(0.17)	1.67(0.19)	1.75(0.19)	1.30(0.14)	1.26(0.14)	1.57(0.17)	1.25(0.14)	1.39(0.15)	1.50	0.19
CO_2 (ppm)	5680(960)	4000(660)	5950(1000)	5040(850)	6750(1090)	5670(940)	4890(790)	4660(780)	5280(880)	7270(1200)	5520	973
CO_2/H_2O	0.34	0.24	0.41	0.30	0.38	0.44	0.39	0.30	0.42	0.52	0.37	N=10

Table C.1. Continued, Sample AW82033

Inclusion	a	b	c	d	e	f	g	h	i	k	l	Mean	StdDev
SiO_2	42.44	43.76	43.24	45.08	43.68	48.34	45.35	42.95	45.00	46.41	46.06	44.75	1.76
TiO_2	3.59	3.66	3.57	3.68	4.18	2.22	3.71	4.25	3.73	3.03	3.54	3.56	0.55
Al_2O_3	17.04	17.89	16.82	16.67	17.71	16.58	19.59	16.92	16.90	17.49	17.39	17.36	0.85
FeO_T	11.86	8.96	9.99	10.23	11.57	11.86	9.66	11.63	11.92	10.93	10.57	10.83	1.02
MnO	0.21	0.15	0.23	0.20	0.18	0.31	0.16	0.21	0.33	0.26	0.25	0.23	0.06
MgO	4.24	3.67	3.24	3.52	4.15	3.06	3.80	4.00	3.58	2.83	3.37	3.59	0.45
CaO	9.98	9.39	10.61	11.22	11.93	6.02	8.70	10.71	8.93	8.26	7.99	9.43	1.69
Na_2O	4.58	4.43	4.99	4.74	4.68	5.81	5.32	4.45	5.00	5.74	5.60	5.03	0.51
K_2O	1.80	2.98	2.00	1.77	1.52	3.69	2.01	1.66	2.65	3.44	3.19	2.43	0.78
P_2O_5	1.22	1.38	1.20	1.40	1.24	1.26	1.37	0.75	1.96	1.30	1.30	1.31	0.28
F (ppm)	1660	740	3240	1860	1840	2720	2080	1590	2130	2790	2810	2133	713
S (ppm)	1405	925	1525	1390	1290	1100	1085	1575	1730	1455	1145	1330	244
Cl (ppm)	750	620	870	870	800	760	750	450	640	1000	1110	784	182
Total	97.34	96.50	96.45	98.93	101.23	99.60	100.05	97.88	100.43	100.22	99.75	98.94	1.65
H_2O (wt%)	0.18(0.02)	0.25(0.03)	0.11(0.02)	0.11(0.02)	0.19(0.03)	0.12(0.02)	0.17(0.02)	0.34(0.05)	0.11(0.02)	0.11(0.02)	0.11(0.02)	0.16	0.07
CO_2 (ppm)	530(110)	290(80)	1650(350)	1240(240)	1940(340)	230(90)	280(110)	930(470)	1330(270)	430(120)	240(300)	825	623
CO_2/H_2O	0.29	0.12	1.49	1.11	1.03	0.18	0.17	0.27	1.16	0.39	0.22	0.50	N=11

Table C.1. Continued, Sample 7713

Inclusion	e	f	g	h	i	j	k	l	Mean	StdDev
SiO_2	47.16	47.80	47.43	47.59	48.51	47.91	47.60	47.74	47.72	0.39
TiO_2	2.66	2.61	2.57	2.63	2.71	2.58	3.10	2.75	2.70	0.17
Al_2O_3	17.47	17.76	18.17	17.96	18.24	17.60	17.42	17.88	17.81	0.31
FeO_T	10.43	10.35	10.16	10.20	10.22	10.68	10.98	10.44	10.43	0.28
MnO	0.26	0.22	0.22	0.22	0.26	0.24	0.30	0.30	0.25	0.03
MgO	2.12	2.35	2.12	2.13	2.31	2.42	2.96	2.04	2.31	0.29
CaO	6.50	6.47	6.63	6.30	6.82	6.62	7.12	7.19	6.71	0.32
Na_2O	6.31	6.25	6.64	6.62	6.72	6.10	4.76	6.25	6.21	0.63
K_2O	3.45	3.55	3.41	3.54	3.41	3.52	3.47	3.58	3.49	0.07
P_2O_5	1.11	1.35	1.07	1.29	1.27	1.54	1.33	1.44	1.30	0.15
F (ppm)	2160	2680	2160	3080	3210	2780	2610	3510	2774	480
S (ppm)	725	1025	1150	825	1095	1440	1305	1310	1109	247
Cl (ppm)	1120	850	1350	1080	820	980	980	1120	1038	170
Total	97.86	99.16	98.89	98.97	100.98	99.73	99.53	100.24	99.42	0.94
H_2O (wt%)	0.12(0.01)	0.10(0.01)	0.12(0.01)	0.11(0.01)	0.09(0.01)	0.11(0.01)	0.14(0.02)	0.08(0.01)	0.11	0.02
CO_2 (ppm)	340(110)	430(120)	490(160)	420(110)	420(100)	510(120)	740(200)	230(80)	448	149
CO_2/H_2O	0.29	0.44	0.40	0.39	0.48	0.45	0.55	0.29	0.42	N=8

Table C.1. Continued, Sample 97009

Inclusion	a	b	c	d	e	f	g	h	i	j	Mean	StdDev
SiO_2	46.92	51.51	51.08	52.02	50.55	50.75	51.83	52.29	52.65	51.48	51.11	1.61
TiO_2	1.79	1.84	1.92	1.80	1.59	2.01	1.50	1.96	1.78	2.01	1.82	0.17
Al_2O_3	18.20	19.40	19.04	19.16	18.95	19.51	19.74	19.65	19.75	19.38	19.28	0.47
FeO_T	6.74	7.19	7.77	7.39	6.58	7.15	6.63	7.50	7.41	7.35	7.17	0.40
MnO	0.24	0.20	0.24	0.21	0.19	0.19	0.18	0.17	0.22	0.20	0.20	0.02
MgO	1.11	1.29	1.29	1.46	1.28	1.28	1.37	1.42	1.26	1.38	1.31	0.10
CaO	3.82	3.67	4.08	4.10	4.06	3.86	4.82	3.67	3.89	3.78	3.97	0.34
Na_2O	7.07	7.50	7.44	7.76	8.57	7.65	7.48	8.14	7.67	7.21	7.65	0.44
K_2O	4.87	4.99	4.79	4.93	5.16	4.93	4.70	4.97	4.79	4.88	4.90	0.13
P_2O_5	0.44	0.44	0.63	0.66	0.63	0.62	0.61	0.50	0.56	0.38	0.55	0.10
F (ppm)	1290	0	1680	1410	0	2210	1720	940	2180	2430	1386	859
S (ppm)	665	635	790	915	525	530	545	610	805	690	671	131
Cl (ppm)	1800	1510	1260	1520	8000	1580	1410	1400	1630	1610	2172	2053
Total	91.56	98.25	98.63	99.88	98.41	98.38	99.22	100.58	100.45	98.51	98.39	2.55
H_2O (wt%)	0.59(0.09)	0.58(0.08)	0.56(0.09)	0.45(0.06)	0.47(0.06)	0.52(0.08)	0.52(0.07)	0.44(0.06)	0.49(0.07)	0.65(0.10)	0.53	0.07
CO_2 (ppm)	3120(450)	1860(290)	2650(430)	1490(260)	1520(270)	2340(370)	2040(310)	3090(470)	2520(330)	3590(600)	2421	707
CO_2/H_2O	0.53	0.32	0.47	0.33	0.32	0.45	0.39	0.70	0.51	0.55	0.46	N=10

Table C.1. Continued, Sample 97010

Inclusion	b	c	d	e	f	g	h	i	Mean	StdDev
SiO_2	53.11	52.53	53.49	54.23	53.30	53.49	53.88	54.46	53.56	0.62
TiO_2	2.04	1.69	2.17	1.66	1.86	1.75	1.86	1.92	1.87	0.17
Al_2O_3	19.10	19.15	18.90	20.14	19.97	19.49	19.92	20.34	19.63	0.54
FeO_T	6.93	7.55	6.82	6.45	6.81	6.75	6.57	5.80	6.71	0.49
MnO	0.23	0.22	0.19	0.19	0.19	0.17	0.18	0.18	0.19	0.02
MgO	1.36	1.24	1.27	1.09	1.31	1.26	1.05	1.14	1.21	0.11
CaO	3.60	3.92	3.74	3.43	3.51	3.31	3.53	3.42	3.56	0.19
Na_2O	8.16	7.51	7.90	8.65	8.05	8.27	7.76	7.77	8.01	0.35
K_2O	5.03	5.15	5.14	5.41	5.25	5.27	5.34	5.17	5.22	0.12
P_2O_5	0.87	0.76	0.77	0.57	0.83	0.83	0.88	0.63	0.77	0.11
F (ppm)	3670	2770	2320	1290	2230	2600	2120	2250	2406	672
S (ppm)	755	540	840	550	345	685	520	695	616	157
Cl (ppm)	1410	1000	1420	1300	1250	1200	1150	1050	1223	154
Total	101.01	100.14	100.82	102.12	101.45	101.03	101.34	101.23	101.14	0.57
H_2O (wt%)	0.12(0.02)	0.11(0.02)	0.13(0.02)	0.13(0.02)	0.13(0.02)	0.12(0.02)	0.11(0.02)	0.10(0.02)	0.12	0.01
CO_2 (ppm)	1950(270)	510(240)	990(180)	ND	740(270)	850(300)	460(140)	650(210)	877	507
CO_2/H_2O	1.62	0.48	0.77		0.57	0.68	0.42	0.65	0.74	N=8

Table C.1. Continued, Sample 97011

Inclusion	a	b	c	d	e	f	Mean	StdDev
SiO_2	52.89	53.29	52.39	55.36	54.86	53.82	53.77	1.15
TiO_2	1.33	1.35	1.25	1.61	1.27	1.25	1.34	0.14
Al_2O_3	19.61	20.33	19.79	20.13	20.08	20.48	20.07	0.32
FeO_T	5.58	5.27	5.51	5.13	5.42	5.69	5.43	0.21
MnO	0.25	0.19	0.17	0.13	0.18	0.25	0.20	0.05
MgO	0.93	0.92	0.99	0.84	0.82	0.87	0.89	0.06
CaO	3.21	3.03	2.64	3.28	3.38	2.93	3.08	0.27
Na_2O	7.51	8.63	8.11	7.95	8.40	8.34	8.16	0.39
K_2O	5.50	5.69	5.30	5.82	5.63	5.57	5.58	0.18
P_2O_5	0.70	0.84	0.62	0.33	0.54	0.47	0.58	0.18
F (ppm)	1770	2270	2260	2440	2000	1470	2035	363
S (ppm)	420	600	515	795	765	670	628	145
Cl (ppm)	1330	1370	1370	1090	1520	1430	1352	144
Total	97.88	99.94	97.19	101.00	101.00	100.03	99.51	1.61
H_2O (wt%)	0.12(0.02)	0.11(0.03)	0.10(0.02)	0.08(0.03)	0.08(0.01)	0.12(0.06)	0.10	0.02
CO_2 (ppm)	1310(130)	670(180)	460(180)	1050(400)	2140(490)	1070(320)	1118	587
CO_2/H_2O	1.13	0.61	0.46	1.28	2.55	0.89	1.10	N=6

Table C.1. Continued, Sample 97006

Inclusion	a	c	d1	d2	Mean	StdDev
SiO_2	54.06	54.33	55.25	54.18	54.46	0.54
TiO_2	1.44	1.29	1.30	1.35	1.35	0.07
Al_2O_3	19.65	19.57	19.68	19.84	19.68	0.11
FeO_T	5.85	5.61	5.67	5.97	5.78	0.16
MnO	0.20	0.22	0.19	0.22	0.21	0.01
MgO	0.91	0.82	0.96	0.92	0.90	0.06
CaO	2.68	2.29	2.32	2.31	2.40	0.19
Na_2O	8.25	8.54	8.71	8.80	8.57	0.24
K_2O	5.30	5.40	5.44	5.28	5.36	0.08
P_2O_5	0.63	0.42	0.39	0.51	0.49	0.11
F (ppm)	2350	2780	1180	1580	1973	725
S (ppm)	490	535	710	895	658	185
Cl (ppm)	1130	1340	1420	1410	1325	135
Total	99.36	98.96	100.24	99.76	99.58	0.55
H_2O (wt%)	0.09(0.01)	0.08(0.01)	0.07(0.01)	0.08(0.01)	0.08	0.01
CO_2 (ppm)	860(270)	1690(430)	980(290)	1130(220)	1166	367
CO_2/H_2O	0.94	1.99	1.40	1.31	1.40	N=4

Table C.1. Continued, Sample 97018

Inclusion	a	b	c	d	e	f	g	Mean	StdDev
SiO_2	55.27	56.50	54.08	56.37	56.02	55.06	56.18	55.64	0.88
TiO_2	0.92	1.06	1.07	0.86	1.03	0.93	0.86	0.96	0.09
Al_2O_3	19.51	20.75	19.57	20.68	20.09	20.32	20.19	20.16	0.49
FeO_T	5.39	5.50	5.35	4.94	5.34	5.50	5.64	5.38	0.22
MnO	0.30	0.24	0.36	0.26	0.23	0.22	0.30	0.27	0.05
MgO	0.85	0.83	0.85	0.80	0.79	0.88	0.86	0.84	0.03
CaO	1.94	2.06	1.85	2.00	1.86	1.77	1.97	1.92	0.10
Na_2O	8.72	9.03	8.60	9.45	8.99	9.10	8.98	8.98	0.27
K_2O	5.56	5.63	5.59	5.69	5.64	5.89	5.50	5.64	0.13
P_2O_5	0.26	0.35	0.26	0.34	0.31	0.22	0.37	0.30	0.05
F (ppm)	2250	2320	1880	2210	2870	1410	2840	2254	513
S (ppm)	225	470	290	335	610	350	290	367	131
Cl (ppm)	1320	1620	1530	1190	1630	1390	1520	1457	163
Total	99.11	102.38	97.95	101.75	100.81	100.20	101.30	100.50	1.55
H_2O (wt%)	0.14(0.01)	0.15(0.02)	0.02(0.003)	0.13(0.01)	0.16(0.02)	0.13(0.01)	0.13(0.01)	0.12	0.05
CO_2 (ppm)	580(260)	620(110)	550(270)	580(220)	810(350)	530(240)	880(390)	650	139
CO_2/H_2O	0.40	0.40	3.58	0.43	0.51	0.40	0.68	0.52	N=7

Table C.1. Continued, Sample EA1

Inclusion	a	b	d	e	f	g	h	i	j	k	Mean	StdDev
SiO_2	55.24	54.79	53.50	55.14	54.55	55.51	54.82	54.43	54.42	55.62	54.83	0.60
TiO_2	1.02	0.91	0.98	0.93	0.93	0.94	0.94	0.96	0.91	0.98	0.95	0.04
Al_2O_3	20.14	20.01	19.30	20.01	19.81	20.06	19.46	19.68	19.68	19.98	19.79	0.28
FeO_T	4.87	4.99	5.04	4.87	5.01	5.03	4.99	5.05	4.98	5.14	4.98	0.10
MnO	0.27	0.21	0.21	0.22	0.28	0.31	0.25	0.25	0.23	0.23	0.25	0.03
MgO	0.85	0.80	0.80	0.82	0.83	0.78	0.85	0.78	0.81	0.84	0.81	0.03
CaO	1.89	1.66	1.86	1.92	1.69	1.96	1.59	1.89	1.91	1.86	1.81	0.12
Na_2O	9.14	8.73	8.25	8.92	9.10	8.89	8.66	8.59	8.65	9.03	8.82	0.27
K_2O	6.12	6.59	6.01	6.23	6.49	6.21	6.83	6.10	5.98	6.12	6.29	0.27
P_2O_5	0.33	0.28	0.29	0.29	0.33	0.31	0.32	0.29	0.32	0.27	0.30	0.02
F (ppm)	2610	2660	2540	2120	3150	2190	2590	2390	3180	2880	2652	347
S (ppm)	335	465	430	365	355	405	395	375	260	420	375	58
Cl (ppm)	1430	1420	1640	1700	1650	1330	1810	1290	1380	1490	1502	171
Total	100.28	99.43	96.69	99.76	99.52	100.38	99.18	98.41	98.37	100.53	99.27	1.11
H_2O (wt%)	0.16(0.02)	0.17(0.02)	0.16(0.02)	0.18(0.02)	0.20(0.02)	0.15(0.02)	0.18(0.02)	0.15(0.02)	0.14(0.01)	0.18(0.02)	0.17	0.02
CO_2 (ppm)	640(340)	730(250)	700(300)	430(190)	640(300)	760(250)	760(300)	790(260)	880(320)	580(270)	690	125
CO_2/H_2O	0.41	0.42	0.44	0.24	0.31	0.50	0.42	0.50	0.61	0.31	0.41	N=10

Table C.2. Matrix Glass Compositions, Sample DVDP 3-283

Analysis	g1	g2	g3	g5	g6	Mean	StdDev
SiO_2	42.93	41.98	41.66	42.36	42.80	42.34	0.54
TiO_2	4.33	4.65	4.28	4.26	4.18	4.34	0.18
Al_2O_3	15.75	15.49	15.94	14.88	15.10	15.43	0.44
FeO_T	9.22	9.39	11.16	9.28	8.61	9.53	0.96
MnO	0.20	0.15	0.18	0.18	0.17	0.17	0.02
MgO	5.56	5.62	5.18	5.71	5.60	5.53	0.20
CaO	12.34	12.96	11.08	13.61	14.07	12.81	1.17
Na_2O	4.20	4.12	4.32	3.40	3.69	3.95	0.39
K_2O	1.84	1.83	2.02	1.58	1.67	1.78	0.17
P_2O_5	0.93	1.05	1.11	0.88	0.92	0.98	0.10
F (ppm)	910	2460	1370	1700	2270	1742	638
S (ppm)	2240	2435	2110	2065	1880	2146	207
Cl (ppm)	850	790	670	710	810	766	74
Total	97.69	97.80	97.34	96.58	97.29	97.34	0.48

Table C.2. Continued, Sample DVDP 3-295

Analysis	1a	1b	2a	2b	3a	3b	Mean	StdDev
SiO_2	42.80	42.27	40.86	41.55	42.30	41.92	41.95	0.68
TiO_2	3.97	4.12	4.12	4.05	4.25	4.24	4.12	0.11
Al_2O_3	15.29	15.46	15.61	15.67	15.89	16.05	15.66	0.28
FeO_T	10.73	11.08	11.14	11.10	11.93	11.77	11.29	0.46
MnO	0.19	0.17	0.19	0.19	0.21	0.19	0.19	0.01
MgO	5.29	5.35	5.20	5.23	4.78	4.97	5.14	0.22
CaO	12.15	12.14	11.73	11.48	10.77	10.97	11.54	0.58
Na_2O	4.40	4.12	3.98	4.68	4.69	4.77	4.44	0.33
K_2O	1.72	1.72	1.82	1.78	2.03	1.96	1.84	0.13
P_2O_5	0.99	1.02	1.06	1.01	1.14	1.10	1.05	0.06
F (ppm)	2070	2020	1510	2200	2190	1350	1890	366
S (ppm)	325	405	840	770	225	465	505	247
Cl (ppm)	840	880	1240	950	1040	1010	993	143
Total	97.84	97.76	96.06	97.12	98.34	98.21	97.56	0.85
H_2O (wt%)	0.26(0.03)		0.34(0.04)		0.23(0.03)			
CO_2 (ppm)	ND		ND		ND			

Number in parentheses represents 2σ uncertainty of FTIR analysis.

Table C.2. Continued, Sample AW82033

Analysis	1a	1b	2a	2b	3a	3b	Mean	StdDev
SiO_2	47.43	48.01	48.58	48.12	48.58	49.33	48.34	0.65
TiO_2	2.82	2.85	2.91	2.77	2.84	2.73	2.82	0.06
Al_2O_3	17.53	17.52	17.52	17.49	17.75	18.06	17.64	0.22
FeO_T	10.20	10.35	10.27	10.46	10.16	10.22	10.28	0.11
MnO	0.22	0.27	0.23	0.26	0.26	0.30	0.26	0.03
MgO	2.73	2.69	2.59	2.67	2.73	2.69	2.68	0.05
CaO	6.30	6.21	6.26	6.40	6.33	6.29	6.30	0.07
Na_2O	6.22	6.15	6.16	6.14	6.30	6.27	6.21	0.07
K_2O	3.82	3.79	3.84	3.88	3.81	3.79	3.82	0.03
P_2O_5	1.27	1.11	1.20	1.08	1.10	1.14	1.15	0.07
F (ppm)	2330	2020	2500	1670	3000	2600	2353	465
S (ppm)	1030	1310	1150	910	990	890	1047	159
Cl (ppm)	820	860	790	940	780	750	823	68
Total	98.95	99.37	100.01	99.61	100.34	101.24	99.92	0.81
H_2O (wt%)	0.10(0.01)		0.010(0.001)		0.10(0.01)			
CO_2 (ppm)	110(50)		10(5)		60(30)			

Table C.2. Continued, Sample 7713

Analysis	1a	1b	2	g1	g2	g3	g4	g5	g6	g7	g8	Mean	StdDev
SiO_2	46.94	47.22	48.29	47.81	47.69	47.64	47.66	47.57	47.89	47.60	48.03	47.67	0.36
TiO_2	2.84	2.82	2.93	3.10	3.14	2.96	3.16	3.00	3.03	3.02	2.93	2.99	0.11
Al_2O_3	17.60	17.56	17.73	17.37	17.44	17.21	17.66	17.39	17.52	17.08	17.37	17.45	0.19
FeO_T	10.27	10.46	10.18	10.56	10.52	10.39	10.19	10.46	10.35	10.41	10.52	10.39	0.13
MnO	0.26	0.22	0.27	0.27	0.28	0.31	0.25	0.27	0.24	0.24	0.30	0.26	0.02
MgO	2.87	2.89	2.87	2.87	2.75	2.72	2.70	2.72	2.74	2.62	2.73	2.77	0.09
CaO	6.53	6.42	6.75	6.67	6.66	6.56	6.53	6.65	6.54	6.58	6.70	6.60	0.10
Na_2O	6.57	6.60	6.56	6.47	6.18	6.47	6.35	6.48	6.48	6.33	6.35	6.44	0.13
K_2O	3.57	3.48	3.90	3.58	3.41	3.56	3.66	3.78	3.77	3.61	3.58	3.63	0.14
P_2O_5	1.14	1.25	1.24	1.41	1.36	1.32	1.20	1.48	1.43	1.46	1.25	1.32	0.11
F (ppm)	3280	1590	2760	3230	1010	4040	3710	3910	2700	0	3500	2703	1301
S (ppm)	1040	1380	1380	1300	865	1315	925	1255	1445	970	1140	1183	204
Cl (ppm)	690	940	860	840	1060	980	800	910	710	1000	810	873	118
Total	99.08	99.32	101.22	100.66	99.72	99.76	99.91	100.40	100.47	99.15	100.33	100.00	0.68
H_2O (wt%)	0.10(0.01)												
CO_2 (ppm)	ND												

Table C.2. Continued, Sample 97006

Analysis	1a	1b	2a	2b	3a	3b	Mean	StdDev
SiO_2	56.09	56.06	54.97	55.26	55.53	55.42	55.55	0.44
TiO_2	1.11	1.08	1.11	1.12	1.11	1.20	1.12	0.04
Al_2O_3	19.69	19.92	19.70	19.53	19.51	19.64	19.66	0.15
FeO_T	5.63	5.70	5.69	5.59	5.84	5.86	5.72	0.11
MnO	0.79	0.80	0.82	0.79	0.87	0.88	0.82	0.04
MgO	0.16	0.26	0.22	0.25	0.24	0.23	0.23	0.04
CaO	1.80	1.80	1.70	1.77	2.00	2.04	1.85	0.14
Na_2O	8.66	9.09	8.86	8.51	8.33	8.54	8.66	0.27
K_2O	6.00	5.99	6.10	6.00	5.81	5.60	5.92	0.18
P_2O_5	0.19	0.27	0.28	0.31	0.21	0.30	0.26	0.05
F (ppm)	1820	2340	2030	3350	2510	1700	2292	602
S (ppm)	405	450	535	360	580	320	442	101
Cl (ppm)	1220	1280	1420	1600	1070	1330	1320	180
Total	100.46	101.38	99.83	99.64	99.86	100.04	100.20	0.64
H_2O (wt%)	0.12(0.01)		0.10(0.01)		0.13(0.02)			
CO_2 (ppm)	320(110)		ND		ND			

Table C.2. Continued, Sample 97009

Analysis	1a	1b	2a	2b	3a	3b	Mean	StdDev
SiO_2	51.91	52.20	52.70	50.65	52.82	53.85	52.36	1.07
TiO_2	1.57	1.55	1.40	1.44	1.64	1.56	1.53	0.09
Al_2O_3	18.97	19.24	19.36	18.77	19.83	20.03	19.37	0.49
FeO_T	7.06	6.84	6.89	6.83	6.84	7.00	6.91	0.10
MnO	0.20	0.21	0.25	0.16	0.26	0.20	0.21	0.04
MgO	1.40	1.31	1.32	1.29	1.37	1.41	1.35	0.05
CaO	3.61	3.59	3.72	3.68	3.72	3.70	3.67	0.06
Na_2O	7.60	7.80	7.78	7.11	8.23	8.32	7.81	0.44
K_2O	4.90	5.01	5.06	4.86	5.00	5.03	4.98	0.08
P_2O_5	0.49	0.44	0.55	0.56	0.48	0.40	0.48	0.06
F (ppm)	1930	1510	1140	1360	1590	2540	1678	497
S (ppm)	520	480	330	505	510	480	471	71
Cl (ppm)	1580	1210	1480	1480	1280	1270	1383	149
Total	98.09	98.50	99.32	95.69	100.53	101.93	99.01	2.15
H_2O (wt%)	0.15(0.02)		0.12(0.01)		0.12(0.01)			
CO_2 (ppm)	170(90)		190(100)		220(120)			

Table C.2. Continued, Sample 97018

Analysis	1a	1a	1b	1b	1c	1c	Mean	StdDev
SiO_2	56.40	55.83	54.84	55.14	55.73	56.22	55.69	0.60
TiO_2	1.08	1.04	0.98	1.04	1.06	1.03	1.04	0.03
Al_2O_3	20.62	20.45	19.87	19.95	20.33	20.53	20.29	0.31
FeO_T	5.81	5.81	5.64	5.71	5.75	5.66	5.73	0.07
MnO	0.26	0.30	0.27	0.39	0.32	0.23	0.29	0.06
MgO	0.89	0.84	0.80	0.81	0.83	0.85	0.84	0.03
CaO	1.99	2.03	1.85	1.81	1.90	1.93	1.92	0.08
Na_2O	9.13	9.05	8.71	8.66	8.98	8.99	8.92	0.19
K_2O	5.66	5.58	5.66	5.57	5.61	5.53	5.60	0.05
P_2O_5	0.33	0.28	0.30	0.32	0.31	0.21	0.29	0.04
F (ppm)	2880	1860	2430	2530	1500	2220	2237	494
S (ppm)	500	490	345	345	505	340	421	85
Cl (ppm)	1700	1670	1460	1230	1780	1630	1578	201
Total	102.67	101.59	99.34	99.82	101.19	101.58	101.03	1.24
H_2O (wt%)	0.07(0.01)							
CO_2 (ppm)	420(50)							

Table D.1. Olivine Analyses with Calculated End-Member Components, Sample DVDP 3-295

Sample	a	b	c	d	g	i	j	l	q	r
SiO_2	39.63	39.06	38.54	38.45	38.54	38.75	40.29	40.17	40.02	38.82
FeO	14.67	13.09	18.25	14.63	14.75	13.34	13.19	14.03	14.11	13.28
MnO	0.11	0.18	0.25	0.27	0.24	0.21	0.24	0.22	0.28	0.22
MgO	46.31	46.49	41.99	42.88	45.21	45.13	45.97	45.80	45.34	45.92
CaO	0.34	0.31	0.26	0.33	0.32	0.36	0.33	0.35	0.32	0.36
Total	101.07	99.13	99.29	96.55	99.05	97.77	100.01	100.56	100.07	98.59
Fa	15.09	13.64	19.60	16.06	15.47	14.22	13.86	14.66	14.87	13.96
Fo	84.91	86.36	80.40	83.94	84.53	85.78	86.14	85.34	85.13	86.04

Table D.1. Continued, Sample DVDP 3-283

Sample	283a	283b	283c	283h
SiO_2	40.47	40.61	40.06	38.59
FeO	14.36	13.82	13.58	18.56
MnO	0.19	0.18	0.24	0.28
MgO	46.52	47.10	46.85	42.09
CaO	0.35	0.34	0.35	0.27
Total	101.89	102.04	101.08	99.78
Fa	14.76	14.13	13.99	19.83
Fo	85.24	85.87	86.01	80.17

Table D.1. Continued, Sample AW 82033

Sample	a	b	c	d	e	f	g	h	j	k	l
SiO_2	38.76	38.29	38.17	38.38	39.35	35.94	38.86	37.19	38.34	39.78	39.45
FeO	22.07	21.34	20.46	23.36	22.39	31.88	19.58	22.82	25.24	16.48	23.58
MnO	0.28	0.26	0.31	0.34	0.27	0.80	0.20	0.36	0.45	0.23	0.41
MgO	40.02	40.18	39.40	38.76	40.79	30.29	42.55	39.74	37.73	44.41	40.34
CaO	0.28	0.30	0.30	0.39	0.28	0.46	0.36	0.36	0.33	0.39	0.42
Total	101.41	100.36	98.64	101.23	103.09	99.36	101.53	100.46	102.09	101.28	104.20
Fa	23.63	22.95	22.56	25.27	23.54	37.13	20.52	24.37	27.29	17.23	24.70
Fo	76.37	77.05	77.44	74.73	76.46	62.87	79.48	75.63	72.71	82.77	75.30

Table D.1. Continued, Sample 7713

Sample	e	f	g	h	i	j	k	l
SiO_2	35.06	35.69	35.99	35.97	36.42	35.80	35.88	35.95
FeO	30.83	31.19	30.65	30.65	30.44	31.54	30.63	30.79
MnO	0.77	0.73	0.64	0.63	0.75	0.73	0.61	0.59
MgO	31.56	32.00	32.52	32.77	33.01	31.46	32.48	32.47
CaO	0.44	0.46	0.45	0.44	0.48	0.45	0.41	0.43
Total	98.65	100.07	100.24	100.46	101.09	99.98	100.01	100.23
Fa	23.81	23.76	23.41	23.38	23.14	23.98	23.44	23.50
Fo	76.19	76.24	76.59	76.62	76.86	76.02	76.56	76.50

Table D.1. Continued, Sample 97006

Sample	a	c	d1	d2
SiO_2	33.69	33.88	33.48	33.52
FeO	37.56	37.39	36.97	37.08
MnO	1.43	1.62	1.53	1.42
MgO	25.93	25.87	26.70	26.65
CaO	0.44	0.46	0.41	0.42
Total	99.05	99.22	99.09	99.08
Fa	27.49	27.37	27.17	27.23
Fo	72.51	72.63	72.83	72.77

Table D.1. Continued, Sample 97009

Sample	a	b	c	d	e	f	g	h	i	j
SiO_2	30.75	34.95	34.97	35.74	35.14	35.51	36.03	35.14	34.82	34.69
FeO	34.08	34.63	34.90	34.54	34.52	34.24	32.04	35.24	34.47	34.15
MnO	0.84	1.06	1.06	0.98	1.02	1.05	0.84	1.04	0.93	0.97
MgO	26.01	27.64	27.78	29.10	28.63	28.48	30.98	28.95	28.54	28.28
CaO	0.43	0.47	0.40	0.45	0.45	0.42	0.37	0.43	0.39	0.40
Total	92.10	98.74	99.11	100.80	99.76	99.69	100.26	100.79	99.14	98.49
Fa	27.01	25.96	26.04	25.52	25.71	25.56	24.22	25.91	25.80	25.74
Fo	72.99	74.04	73.96	74.48	74.29	74.44	75.78	74.09	74.20	74.26

Table D.1. Continued, Sample 97010

Sample	b	c	d	e	f	g	h	i
SiO_2	36.83	35.65	36.25	36.37	36.10	36.63	35.87	35.97
FeO	31.31	33.23	31.25	33.85	32.07	31.60	32.01	31.46
MnO	1.08	1.07	0.96	1.23	0.95	0.97	0.98	1.07
MgO	31.53	29.02	31.61	29.65	30.79	31.76	31.37	30.82
CaO	0.42	0.41	0.41	0.40	0.38	0.38	0.35	0.38
Total	101.16	99.38	100.48	101.49	100.28	101.33	100.59	99.70
Fa	35.78	39.12	35.68	39.04	36.88	35.82	36.40	36.41
Fo	64.22	60.88	64.32	60.96	63.12	64.18	63.60	63.59

Table D.1. Continued, Sample 97011

Sample	a	b	c	d	e	f
SiO_2	33.75	35.72	35.76	36.31	35.66	35.86
FeO	33.26	33.32	29.99	32.90	33.99	33.72
MnO	1.19	1.11	0.99	1.07	1.16	1.17
MgO	28.11	29.62	29.92	30.56	29.40	29.08
CaO	0.39	0.38	0.40	0.44	0.38	0.35
Total	96.70	100.15	97.06	101.27	100.59	100.18
Fa	25.59	24.96	23.61	24.52	25.26	25.18
Fo	74.41	75.04	76.39	75.48	74.74	74.82

Table D.1. Continued, Sample 97018

Sample	1a	1b	2a	2b	3a	3b	4a	4b	5a	5b
SiO_2	34.53	34.40	33.90	34.28	34.46	34.35	33.69	33.54	33.57	33.96
FeO	39.05	38.69	38.98	38.79	38.76	38.64	39.01	38.06	39.01	39.02
MnO	2.26	2.41	2.34	2.54	2.38	2.39	2.43	2.39	2.29	2.36
MgO	23.77	23.66	23.61	23.78	23.96	23.90	23.78	23.96	23.63	23.96
CaO	0.54	0.51	0.46	0.50	0.46	0.49	0.50	0.49	0.43	0.47
Total	100.14	99.67	99.29	99.88	100.02	99.77	99.41	98.43	98.92	99.77
Fa	28.06	27.96	28.19	27.97	27.93	27.91	28.18	27.88	28.28	28.11
Fo	71.94	72.04	71.81	72.03	72.07	72.09	71.82	72.12	71.72	71.89

Table D.2. Analyses of Pyroxenes with Calculated End-Member Components, Sample DVDP 3-295

Sample[a]	1a	1b	2a	2b	3a	3b	4a	4b	5a	5b
SiO_2	44.73	49.54	44.94	48.84	47.23	48.04	48.70	44.37	46.92	46.80
TiO_2	3.13	1.52	3.19	2.15	2.34	2.42	1.49	4.05	2.23	3.21
Al_2O_3	9.01	4.76	8.99	4.29	7.15	5.63	5.14	8.83	7.04	6.32
FeO_T	6.56	4.89	6.81	5.48	5.60	5.61	8.71	6.27	5.51	6.85
MnO	0.08	0.12	0.13	0.11	0.12	0.07	0.23	0.07	0.08	0.11
MgO	12.23	15.32	12.24	14.76	13.72	14.22	12.80	12.45	13.49	13.31
CaO	21.79	22.87	22.40	23.23	22.47	23.33	21.91	23.29	22.60	22.80
Na_2O	0.73	0.50	0.78	0.33	0.63	0.39	0.98	0.45	0.53	0.41
Cr_2O_3	0.18	0.81	0.27	0.45	0.22	0.55	0.02	0.56	0.93	0.06
Total	98.43	100.35	99.74	99.64	99.48	100.27	99.97	100.37	99.33	99.88
Wo[b,1]	49.54	47.55	49.94	48.27	48.82	49.06	46.93	51.12	49.42	48.76
En[c,1]	38.68	44.32	37.98	42.68	41.48	41.62	38.14	38.02	41.04	39.62
Fs[d,1]	11.78	8.14	12.08	9.05	9.70	9.32	14.94	10.86	9.54	11.62

[a] Numbers ending "a" are grain cores, those ending "b" are rims. [b] Wo = Wollastinite. [c] En = Enstatite. [d] Fs = ferrosilite.
[1] End-members calculated after Cawthorn and Collerson, (1974).

Table D.2. Continued, Sample DVDP 3-283

Sample[a]	1a	1b	2a	2b	3a	3b	4a	4b	5a	5b
SiO_2	46.55	46.98	44.98	48.13	43.48	49.12	44.14	49.27	46.56	48.01
TiO_2	2.39	2.08	3.02	1.85	3.81	1.81	3.75	2.13	2.65	2.06
Al_2O_3	7.69	6.74	8.85	5.96	10.27	5.39	9.48	4.66	7.88	6.38
FeO_T	7.22	4.98	7.13	4.88	7.10	5.30	6.97	5.35	6.17	6.59
MnO	0.11	0.07	0.15	0.07	0.14	0.04	0.11	0.11	0.14	0.14
MgO	12.71	13.83	12.08	14.37	11.88	14.55	11.96	14.88	13.16	13.75
CaO	22.08	22.54	21.91	22.97	22.04	22.49	22.10	23.36	22.42	22.38
Na_2O	0.81	0.56	0.78	0.50	0.72	0.55	0.78	0.32	0.66	0.66
Cr_2O_3	0.14	1.12	0.23	0.99	0.18	0.44	0.05	0.40	0.16	0.12
Total	99.72	98.89	99.12	99.72	99.59	99.71	99.35	100.48	99.81	100.07
Wo[b,1]	48.54	49.30	49.35	49.06	49.85	47.95	49.94	48.33	49.10	47.86
En[c,1]	38.88	42.08	37.86	42.69	37.38	43.16	37.59	42.85	40.11	40.91
Fs[d,1]	12.58	8.62	12.79	8.25	12.77	8.89	12.47	8.82	10.79	11.23

Table D.2. Continued, Sample AW82033

Sample[a]	1a	1b	2a	2b	3b	4a	4b	5a	5b
SiO_2	48.57	43.54	45.94	45.66	46.94	46.18	47.37	46.02	45.22
TiO_2	1.89	3.91	2.58	2.50	2.91	2.51	1.77	2.47	3.05
Al_2O_3	5.56	8.36	7.85	7.78	5.68	8.16	6.13	7.30	9.20
FeO_T	4.94	6.04	5.57	5.68	6.48	5.82	5.28	6.10	6.62
MnO	0.06	0.07	0.11	0.12	0.11	0.10	0.09	0.11	0.11
MgO	14.71	12.07	13.07	13.00	13.94	13.10	13.75	12.83	12.49
CaO	23.05	22.93	22.46	22.29	22.84	22.20	22.11	22.27	22.20
Na_2O	0.45	0.40	0.92	0.30	0.45	0.61	0.80	0.64	0.81
Cr_2O_3	0.39	0.71	0.59	0.54	0.20	0.62	0.94	0.20	0.23
Total	99.62	98.03	99.10	97.87	99.59	99.28	98.25	97.96	99.94
$Wo^{b,1}$	48.61	51.54	49.83	49.64	48.21	49.28	48.65	49.52	49.52
$En^{c,1}$	43.17	37.75	40.34	40.28	40.93	40.46	42.11	39.70	38.77
$Fs^{d,1}$	8.22	10.72	9.84	10.08	10.86	10.26	9.24	10.78	11.71

Table D.2. Continued, Sample 97006

Sample[a]	1a	1b	2a	-2b	3a	3b	4a	4b	5a	5b
SiO_2	50.17	49.33	50.54	50.54	49.76	50.18	50.45	50.01	49.73	49.31
TiO_2	1.49	1.68	1.50	1.52	1.57	1.58	1.36	1.51	1.53	2.06
Al_2O_3	2.85	3.18	3.03	2.82	3.04	3.14	2.47	2.62	3.23	3.74
FeO_T	9.66	9.56	10.01	9.62	9.75	9.83	9.44	9.56	9.86	9.76
MnO	0.55	0.55	0.56	0.53	0.58	0.51	0.47	0.52	0.57	0.48
MgO	12.55	12.27	12.22	12.43	12.27	12.32	12.53	12.37	12.18	12.12
CaO	21.35	21.25	20.87	21.27	21.43	21.00	21.66	21.52	20.88	21.53
Na_2O	1.12	0.84	1.03	0.86	0.93	0.00	0.85	0.91	1.02	0.86
Cr_2O_3	0.00	0.00	0.00	0.01	0.00	0.00	0.02	0.00	0.00	0.01
Total	99.75	98.66	99.76	99.61	99.33	98.57	99.25	99.02	99.01	99.89
$Wo^{b,1}$	45.64	45.98	45.24	45.75	46.02	45.44	46.25	46.19	45.42	46.41
$En^{c,1}$	37.33	36.94	36.86	37.20	36.65	37.09	37.23	36.93	36.87	36.34
$Fs^{d,1}$	17.03	17.08	17.90	17.06	17.33	17.48	16.53	16.88	17.72	17.25

Table D.2. Continued, Sample 97009

Sample[a]	1a	1b	2a	2b	3a	3b	4a	4b	5a	5b
SiO_2	46.07	47.73	47.99	47.40	46.79	47.20	49.37	48.68	48.93	48.43
TiO_2	3.37	2.39	2.41	2.58	2.80	2.54	1.78	2.37	2.05	2.25
Al_2O_3	6.56	5.07	5.40	5.54	6.09	5.58	3.60	5.33	4.53	5.00
FeO_T	9.36	8.97	8.92	8.88	9.19	9.11	8.78	8.76	8.89	9.05
MnO	0.36	0.32	0.35	0.32	0.33	0.33	0.35	0.31	0.30	0.34
MgO	10.81	11.66	11.90	11.53	11.26	11.56	12.64	12.15	12.25	12.02
CaO	21.89	21.61	21.87	21.69	21.93	21.00	21.99	21.71	21.52	21.75
Na_2O	0.90	0.85	0.86	0.83	0.83	0.88	0.75	0.94	0.87	0.86
Cr_2O_3	0.01	0.00	0.00	0.01	0.00	0.00	0.00	0.02	0.00	0.00
Total	99.34	98.61	99.70	98.80	99.22	98.23	99.26	100.29	99.33	99.69
$Wo^{b,1}$	49.17	47.94	47.90	48.28	48.69	47.24	47.07	47.50	47.05	47.47
$En^{c,1}$	33.79	35.98	36.26	35.72	34.80	36.17	37.65	37.00	37.26	36.53
$Fs^{d,1}$	17.04	16.09	15.85	16.00	16.50	16.59	15.27	15.51	15.69	16.00

Table D.2. Continued, Sample 97010

Sample[a]	1a	1b	2a	2b	3a	3b	4a	4b	5a	5b
SiO_2	50.21	49.20	47.65	47.54	49.30	46.99	47.68	47.94	50.08	49.62
TiO_2	1.56	1.85	2.40	2.42	1.91	2.58	2.30	1.99	1.62	1.96
Al_2O_3	2.58	4.03	5.24	4.76	4.24	5.48	4.92	4.40	3.46	4.18
FeO_T	8.24	8.00	8.76	8.49	9.05	9.40	8.84	9.08	8.60	8.92
MnO	0.39	0.36	0.38	0.35	0.38	0.39	0.35	0.40	0.39	0.36
MgO	13.14	13.17	12.10	12.44	12.56	11.39	12.39	12.21	13.11	12.83
CaO	22.51	22.18	21.26	21.76	21.13	21.00	21.26	20.97	21.46	20.91
Na_2O	0.82	0.79	1.00	0.82	1.03	1.16	0.99	1.07	0.88	1.00
Cr_2O_3	0.06	0.00	0.01	0.00	0.00	0.03	0.00	0.00	0.02	0.00
Total	99.51	99.59	98.82	98.59	99.60	98.43	98.73	98.06	99.65	99.78
Wo[b,1]	47.36	47.15	47.00	47.32	45.96	47.20	46.55	46.24	45.92	45.45
En[c,1]	38.46	38.97	37.22	37.66	38.02	35.62	37.74	37.44	39.05	38.79
Fs[d,1]	14.18	13.88	15.78	15.02	16.02	17.18	15.71	16.32	15.04	15.75

Table D.2. Continued, Sample 97011

Sample[a]	1a	2a	2b	3a	3b	4a	4b	5a	5b
SiO_2	49.01	48.47	49.10	48.36	47.06	48.10	48.10	49.46	48.34
TiO_2	2.03	2.13	1.96	2.16	2.61	2.57	2.36	1.97	2.10
Al_2O_3	4.74	4.48	4.46	4.19	5.44	5.11	4.81	4.14	4.71
FeO_T	9.16	8.84	9.41	8.70	8.91	8.91	8.96	9.22	9.07
MnO	0.45	0.33	0.39	0.34	0.35	0.37	0.40	0.37	0.43
MgO	12.10	12.48	12.13	12.44	11.57	11.98	11.87	12.36	11.74
CaO	20.37	21.40	20.84	21.56	21.63	21.91	21.07	21.03	21.06
Na_2O	1.18	1.04	1.16	0.96	1.05	0.96	1.08	1.08	1.08
Cr_2O_3	0.00	0.00	0.00	0.00	0.01	0.00	0.01	0.02	0.00
Total	99.07	99.19	99.45	98.71	98.63	99.92	98.67	99.66	98.53
$Wo^{b,1}$	45.57	46.60	45.94	46.94	48.11	47.81	46.93	46.01	47.00
$En^{c,1}$	37.64	37.81	37.19	37.70	35.81	36.37	36.79	37.60	36.46
$Fs^{d,1}$	16.79	15.59	16.87	15.37	16.08	15.82	16.28	16.39	16.54

Table D.2. Continued, Sample 97018

Sample[a]	1a	1b	2a	2b	3a	3b	4a	4b	5a	5b
SiO_2	49.82	49.39	49.49	49.34	49.52	49.24	49.06	49.08	49.42	48.90
TiO_2	1.56	1.36	1.30	1.23	1.29	1.23	1.38	1.62	1.34	1.54
Al_2O_3	3.14	2.74	2.49	2.66	2.67	2.40	2.91	3.50	3.00	3.45
FeO_T	10.04	9.65	9.94	10.36	9.97	9.60	9.92	10.15	9.85	10.56
MnO	0.67	0.65	0.68	0.66	0.65	0.67	0.69	0.70	0.68	0.66
MgO	11.81	12.28	12.24	11.72	12.08	12.33	11.77	11.65	12.18	11.52
CaO	21.06	21.21	21.31	20.86	21.23	21.58	20.81	20.38	20.94	20.15
Na_2O	1.13	1.03	0.97	1.15	1.02	0.88	1.11	1.27	1.07	1.22
Cr_2O_3	0.00	0.00	0.01	0.04	0.00	0.00	0.00	0.01	0.03	0.01
Total	99.25	98.31	98.42	98.02	98.43	97.93	97.67	98.37	98.53	98.01
$Wo^{b,1}$	45.92	45.76	45.69	45.58	45.82	46.15	45.76	45.23	45.41	44.83
$En^{c,1}$	35.83	36.88	36.52	35.63	36.28	36.70	36.00	35.97	36.74	35.67
$Fs^{d,1}$	18.25	17.36	17.79	18.79	17.90	17.15	18.24	18.81	17.85	19.51

Table D.3. Feldspar Analyses and Calculated End-Member Components

Sample	97018a	97018b	97018c	97018d	97018e	97018f	97018g
SiO_2	62.10	63.37	61.90	63.69	63.24	62.65	63.64
Al_2O_3	23.02	23.42	22.68	23.85	23.20	22.92	22.98
FeO	0.22	0.23	0.20	0.19	0.17	0.22	0.20
CaO	3.70	3.53	3.33	3.58	3.53	3.29	3.01
Na_2O	7.56	7.67	7.52	8.04	7.73	7.66	7.83
K_2O	2.72	2.96	3.05	2.93	2.90	3.15	3.38
Total	99.30	101.17	98.69	102.28	100.77	99.89	101.04
Ab	66.36	66.32	66.13	67.28	66.71	66.31	66.81
An	17.94	16.85	16.20	16.56	16.82	15.75	14.20
Or	15.70	16.83	17.67	16.16	16.47	17.94	18.99

Table D.3. Continued, Sample EA1

Sample	EA1a	EA1c	EA1d	EA1e	EA1f	EA1g	EA1h	EA1i	EA1j	EA1k
SiO_2	62.04	62.10	60.91	62.23	62.19	61.81	61.87	60.67	60.85	62.60
Al_2O_3	23.30	23.32	22.75	23.58	23.36	23.40	23.03	22.84	22.98	23.45
FeO	0.19	0.19	0.22	0.21	0.21	0.17	0.21	0.25	0.21	0.17
CaO	3.86	4.05	3.89	3.95	3.77	4.06	4.00	4.01	4.31	3.93
Na_2O	7.72	7.71	7.28	7.70	7.72	7.72	7.62	7.29	7.51	7.92
K_2O	2.66	2.51	2.58	2.52	2.77	2.65	2.64	2.58	2.25	2.70
Total	99.77	99.88	97.63	100.19	100.02	99.81	99.37	97.62	98.12	100.76
Ab	66.53	66.44	65.43	66.72	66.39	65.96	65.88	65.07	66.03	66.76
An	18.39	19.31	19.31	18.90	17.91	19.18	19.10	19.76	20.95	18.28
Or	15.08	14.25	15.26	14.38	15.70	14.87	15.01	15.17	13.01	14.95

Table D.3. Continued, Sample 7713

Sample	7713a	7713b	7713c	7713d
SiO_2	50.83	54.20	54.28	50.93
Al_2O_3	28.82	29.45	28.65	29.46
FeO	0.39	0.30	0.30	0.34
CaO	11.44	10.68	10.11	12.00
Na_2O	4.21	5.14	5.37	4.11
K_2O	0.54	0.65	0.71	0.47
Total	96.22	100.42	99.41	97.31
Ab	38.66	44.82	47.01	37.20
An	58.07	51.43	48.89	60.03
Or	3.26	3.75	4.10	2.77

Table D.3. Continued, Sample AW82033

Sample	AW82033-1	AW82033-2	AW82033-3	AW82033-4	AW82033-5	AW82033-6
SiO_2	54.06	54.77	53.85	54.42	54.88	54.94
Al_2O_3	28.91	28.25	28.85	27.98	28.06	27.88
FeO	0.28	0.32	0.32	0.35	0.36	0.33
CaO	10.80	10.07	10.79	10.17	9.89	9.94
Na_2O	4.85	5.03	4.87	5.16	5.23	5.24
K_2O	0.67	0.71	0.62	0.71	0.75	0.76
Total	99.57	99.15	99.30	98.78	99.17	99.09
Ab	43.06	45.47	43.34	45.87	46.72	46.65
An	53.02	50.29	53.04	49.97	48.84	48.89
Or	3.92	4.23	3.62	4.16	4.43	4.47

Table D.4. Spinel Grains in Melt Inclusions

Sample	TiO_2	Al_2O_3	Cr_2O_3	FeO	Fe_2O_3	MnO	MgO	CaO	Total
295d	3.183	25.973	23.77	17.607	12.74	0.271	12.965	0.141	96.65
295g	4.117	24.126	20.563	19.71	17.493	0.387	12.282	0.138	98.816
295p	3.503	22.408	26.555	20.722	13.79	0.35	11.09	0.094	98.512
7713f	22.977	4.592	0.008	44.672	20.897	0.578	4.884	0.127	98.735
97006a	25.498	2.028	0.014	48.467	17.452	1.234	3.045	0.081	97.819
97006c	25.95	2.056	0.003	49.272	17.328	1.327	2.974	0.057	98.967
97006d1	26.753	2.267	0	49.816	16.275	1.305	3.307	0.06	99.783
97009e	26.008	3.919	0.004	48.904	16.291	0.844	3.987	0.036	99.993
97009g	51.855	0.42	0.031	40.744	0	0.847	4.809	0.192	98.898
97010c	17.049	2.85	0.01	27.556	37.232	1.09	11.648	0.18	97.615
97010d	23.989	3.363	0	46.183	21.857	1.069	4.533	0.093	101.087
97010i	23.864	3.643	0.003	46.579	21.843	0.977	4.345	0.07	101.324
97011d	24.334	3.717	0.055	47.496	20.736	1.07	4.014	0.073	101.495
97011e	24.144	2.986	0.017	48.099	21.151	0.896	3.39	0.18	100.863
AW82033c	19.618	9.19	0.09	37.367	19.283	0.295	7.185	0.051	93.079
AW82033f	20.678	4.239	0.035	44.296	26.803	0.667	4.082	0.058	100.858

Table D.5. Apatite Crystals in Melt Inclusions

Sample	P_2O_5	CaO	FeO	F	Cl	Total
7713e	42.01	52.25	0.70	4.15	0.17	99.28
7713g	42.09	52.36	0.71	5.55	0.20	100.91
7713h	41.71	52.28	0.96	5.48	0.21	100.64
7713i	40.93	51.49	0.95	5.07	0.22	98.66
7713j	42.01	54.82	0.92	4.25	0.18	102.18
7713k	41.90	52.54	0.64	5.33	0.20	100.61
97006c	41.31	52.69	0.58	5.31	0.14	100.04
97006d1	40.93	52.80	0.92	5.46	0.17	100.29
97006d2	41.73	51.54	0.88	5.58	0.17	99.91
97009b	41.30	54.35	0.73	2.63	0.19	99.19
97009i	41.06	51.48	1.30	3.66	0.22	97.71
97009j	41.81	54.32	0.69	4.01	0.20	101.02
97010d	41.46	54.03	0.87	5.29	0.23	101.88
97011d	41.51	54.41	0.66	4.37	0.22	101.16
AW82033i	42.24	54.02	0.54	4.24	0.16	101.20

Table E.1. Ion Probe Analyses of Selected Melt Inclusions

Sample	Li	B	F	Rb	Sr	Y	Zr	Nb	Ba	Ce	Nd	Eu	Tb	Tm	Th
295A	6.5	5.3	2122	42	1002	35	477	110	625	165	74	4.2	1.2	0.8	10.7
295B	6.5	6.5	2028	39	1023	41	514	107	517	169	67	2.5	2.3	0.6	9.0
295D	10.1	8.1	1909	37	995	39	456	99	538	163	75	3.4	1.8	0.7	9.4
295G	6.8	4.3	1755	36	955	37	451	101	487	150	73	3.6	1.9	0.7	8.2
295J	7.0	4.6	2019	36	1021	37	458	103	545	164	67	3.7	2.0	0.6	8.2
295L	6.4	4.6	1907	38	1004	35	456	97	527	156	67	3.2	1.8	0.5	8.4
295Q	6.7	6.8	2014	38	1024	39	479	103	545	163	65	2.7	1.7	0.9	10.9
295R	7.7	5.1	1728	39	1019	36	446	101	532	161	69	3.0	1.3	0.9	8.6
AW82033B	5.2	6.8	1372	50	644	29	550	160	737	211	81	3.5	1.3	0.5	12.8
AW82033H	7.1	4.2	1849	31	1241	40	386	73	529	132	61	3.0	2.0	1.1	6.5
AW82033I	11.7	5.8	1281	43	1043	68	508	138	615	399	142	6.7	3.2	0.9	16.0
AW82033K	13.8	6.9	2412	59	860	48	617	166	830	235	93	5.1	2.2	1.2	16.0
7713E	15.5	8.0	2860	72	976	47	684	217	1078	254	99	4.4	1.8	1.2	18.5
7713G	14.7	8.0	2662	61	940	48	627	175	854	220	72	n.r.	n.r.	n.r.	n.r.
7713H	14.6	13.8	2105	60	859	45	613	172	839	212	74	5.0	2.3	0.7	12.8
7713L	13.8	7.5	2237	60	922	56	662	200	1030	286	100	5.3	2.1	1.1	17.2

All elements expressed in ppm. n.r. = not recorded

Table E.1. Continued

Sample	Li	B	F	Rb	Sr	Y	Zr	Nb	Ba	Ce	Nd	Eu	Tb	Tm	Th
97009B	23.2	11.0	2032	99	673	41	853	275	1090	213	72	3.0	2.0	0.7	24.5
97009C	21.9	10.2	2235	85	710	44	822	266	1088	248	77	3.8	2.3	0.7	22.4
97009D	23.0	10.5	2704	82	658	41	811	248	1006	230	75	4.6	1.8	1.1	19.2
97009J	26.2	9.7	1837	90	682	39	841	262	1073	214	70	2.6	2.1	1.2	24.9
97010B	23.6	11.1	2219	102	638	45	966	246	968	244	84	4.4	2.0	0.5	19.4
97010C	25.3	10.8	2714	103	551	48	1001	278	995	249	85	4.5	2.2	1.1	25.2
97010D	21.3	12.3	1739	88	589	49	942	273	959	280	93	4.4	2.2	1.3	25.3
97010G	25.5	11.8	2265	117	506	47	1036	275	877	245	82	5.0	3.0	0.9	29.4
97011D	30.0	12.7	2093	99	453	43	1030	264	1008	224	70	2.4	1.7	1.0	24.8
97011E	28.9	13.3	2386	107	580	47	1080	289	1019	254	72	3.0	2.4	1.1	31.5
97006C	27.6	15.6	2630	118	313	55	1266	311	750	266	85	3.6	2.9	1.1	27.1
97006D1	32.2	15.0	2044	122	303	55	1274	325	699	284	93	3.7	2.6	0.9	28.4
97018A	44.4	18.8	2730	133	284	62	1598	426	650	316	99	4.3	3.3	1.6	46.7
97018C	41.6	16.7	2077	117	284	61	1340	342	607	279	83	3.3	3.5	1.3	30.3
97018E	39.3	15.5	2468	119	271	63	1485	407	769	384	116	4.5	3.7	1.7	40.1

Table E.2. Water Analyses SIMS vs. FTIR

Sample	SIMS[1]	SIMS[2]	FTIR
DVDP 3-295B	0.84 (0.13)	1.56 (0.23)	1.67 (0.18)
DVDP 3-295D	0.66 (0.10)	1.26 (0.19)	1.67 (0.19)
DVDP 3-295G	0.91 (0.14)	1.67 (0.25)	1.75 (0.19)
DVDP 3-295J	0.98 (0.15)	1.80 (0.27)	1.26 (0.14)
DVDP 3-295L	0.77 (0.12)	1.45 (0.22)	1.57 (0.17)
DVDP 3-295Q	0.55 (0.08)	1.08 (0.16)	1.25 (0.14)
DVDP 3-295R	0.64 (0.10)	1.22 (0.18)	1.39 (0.15)
C.F.	0.20	0.12	

[1] Water concentrations based on calibration factor for basalt.
[2] Water concentration based on calibration factor for kaersutite.
C.F. = calibration factor.

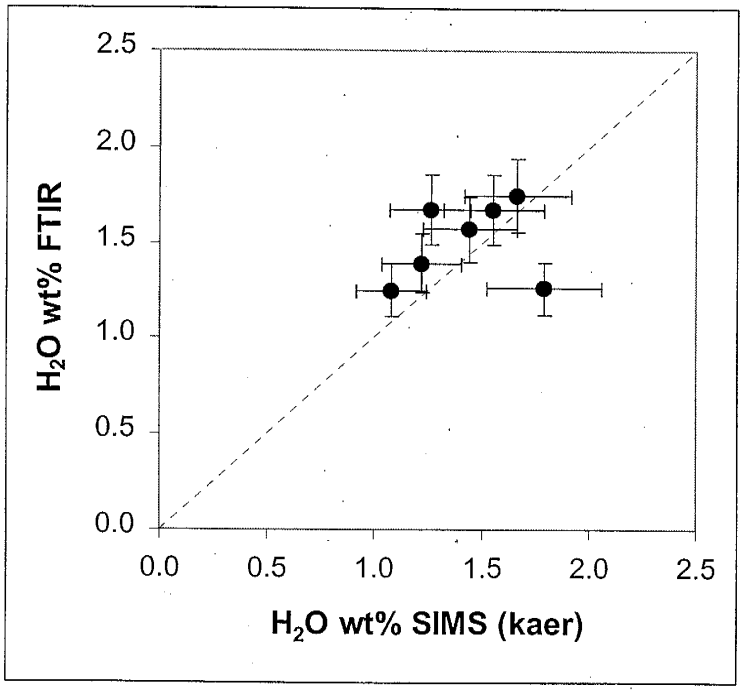

Figure E.1. FTIR versus SIMS (kaersutite calibration) water measurements. Error bars represent 2σ uncertainty.

Table F.1. X-ray Fluorescence Bulk Rock Analyses

Sample	DVDP 3-283	DVDP 3-295	AW82033	7713	97006	97009	97010A	97010B	97010C	97011	97018A	97018B
SiO_2	41.24	38.85	45.92	47.41	53.54	50.69	51.01	50.38	51.21	49.38	56.41	56.04
TiO_2	3.43	3.08	3.01	2.79	1.60	1.97	1.95	1.93	1.97	2.21	0.99	0.98
Al_2O_3	12.81	11.06	17.05	18.53	18.95	18.59	19.51	19.39	19.51	18.61	19.91	19.73
Fe_2O_3	11.67	11.58	11.37	10.52	7.41	9.04	7.78	7.72	7.85	8.72	5.35	5.34
MnO	0.18	0.17	0.22	0.22	0.23	0.23	0.20	0.19	0.20	0.21	0.23	0.23
MgO	10.91	12.43	3.89	2.79	1.53	1.92	2.05	2.06	2.05	2.45	0.87	0.88
CaO	11.61	9.89	8.06	7.59	4.13	4.46	5.45	5.41	5.50	5.60	2.68	2.67
Na_2O	2.91	2.53	5.11	5.86	7.25	7.58	6.93	6.88	6.94	6.54	8.38	8.37
K_2O	1.10	1.14	2.54	2.75	3.84	4.27	3.36	3.30	3.42	3.35	4.54	4.47
P_2O_5	0.71	0.63	1.09	1.21	0.73	0.82	0.97	0.96	0.98	1.09	0.41	0.41
L.O.I.	0.33	6.50	1.03	-0.03	0.33	0.09	0.00	0.00	0.00	-0.56	-0.16	-0.16
SUM	97.16	98.14	99.59	99.99	99.87	99.96	99.55	98.56	99.98	97.92	99.93	99.29
V	275	253	137	79	22.8	26.6	42.7	46.7	45.1	66.8	9.8	7.1
Cr	601	620	50	<10	<10	<10	<10	<10	<10	<10	<10	<10
Ni	210	249	23.3	8.2	5.1	5.5	5.3	5.1	4.6	6.6	4.5	4.4
Cu	71.3	79.7	42.0	41.0	6.3	17.9	12.6	10.2	12.2	12.8	5.0	4.0
Zn	91	90	116	115	119	113	97	96	97	104	127	127
Ga	18.6	16.4	22.1	22.0	24.3	21.9	22.2	20.7	21.5	23.9	27.4	27.0
Rb	21.8	21.5	45	58	87	99	73	73	73	74	107	106
Sr	807	720	1059	1316	1200	812	1321	1321	1324	1309	911	916
Y	29.4	26.0	43.0	42.3	49.9	45.4	39.8	38.5	39.9	43.0	55.5	56.3
Zr	320	286	470	486	795	749	636	633	634	651	1016	1015
Nb	69	62	129	146	202	234	168	168	168	171	261	261
Mo	4.9	3.0	4.9	6.5	9.8	10.4	7.4	8.2	7.9	8.2	12.1	12.0
Ba	426	360	672	773	1028	900	833	817	829	838	1121	1136
Pb	6.1	4.1	5.9	6.4	6.3	7.0	5.7	6.2	4.9	6.1	5.3	6.3
Th	12.8	10.9	16.2	18.0	23.4	23.7	21.5	21.1	19.9	21.7	26.6	26.1
U	2.8	3.9	3.9	3.3	6.0	6.5	5.5	4.1	5.0	6.2	6.6	6.8

L.O.I. = Loss on ignition

Table G.1. Electron Microprobe Standard Analyses

	KE-12	KN-18	VG-2	Bee-Apat	Anorthite	USNM-Ol	Diopside
N	71	22	67	11	18	46	10
SiO_2	70.72 (0.55)	74.57 (0.33)	50.55 (0.40)		44.29 (0.36)	40.42 (0.77)	55.38 (0.23)
TiO_2	0.30 (0.03)	0.18 (0.03)	1.89 (0.06)				0.01 (0.01)
Al_2O_3	7.84 (0.14)	10.84 (0.16)	14.05 (0.28)		36.00 (0.32)		0.04 (0.01)
FeO_T	8.59 (0.18)	3.53 (0.07)	12.00 (0.19)	0.02 (0.02)	0.38 (0.03)	9.84 (0.13)	0.06 (0.02)
MnO	0.28 (0.03)	0.06 (0.02)	0.22 (0.03)			0.13 (0.04)	0.01 (0.02)
MgO	0.01 (0.01)	0.00 (0.01)	6.82 (0.11)			49.30 (0.40)	18.56 (0.07)
CaO	0.37 (0.03)	0.15 (0.04)	10.85 (0.17)	53.61 (0.52)	18.91 (0.15)	0.11 (0.01)	26.15 (0.17)
Na_2O	6.73 (0.64)	5.17 (0.35)	2.76 (0.08)		0.68 (0.04)		0.03 (0.04)
K_2O	4.35 (0.09)	4.52 (0.07)	0.21 (0.02)		0.02 (0.01)		0.01 (0.01)
P_2O_5	0.02 (0.02)	0.01 (0.01)	0.23 (0.04)	40.49 (0.26)			
F	0.45 (0.12)	0.66 (0.06)	0.07 (0.07)	5.87 (0.47)			
S	0.02 (0.01)	0.01 (0.01)	0.15 (0.02)				
Cl	0.29 (0.02)	0.31 (0.01)	0.03 (0.01)	0.01 (0.01)			

Numbers in parentheses represent 1 standard deviation.

Table G.2. Accepted Values for Electron Microprobe Standards

Standard	KE-12[1]	KN-18[1]	VG-2[2] (NIST)	Beeson Apatite[3]	Anorthite[4] (UC#16706)	USNM-Ol[2] (Fo 90)	Diopside[4] (Chesterman)
SiO_2	70.30	74.60	50.81		44.17	40.81	55.47
TiO_2	0.33	0.18	1.85				
Al_2O_3	7.62	10.53	14.06		34.95		0.03
FeO_T	8.60	3.45	11.84	0.04	0.57	9.55	0.06
MnO	0.26	0.06	0.22			0.14	
MgO	0.02	0.01	6.71			49.42	18.56
CaO	0.35	0.15	11.12	54.31	18.63	<0.05	25.87
Na_2O	7.28	5.68	2.62		0.79		0.02
K_2O	4.27	4.39	0.19		0.05		
P_2O_5	0.02	0.01	0.20	40.93			
F	0.42	0.64		3.67			
S							
Cl	0.33	0.37					

[1] H.Sigurdsson (pers. comm.) [2] Jarosewich et al. (1980) [3] S.T. Neil (pers. comm.) [4] Donovan (pers. comm.)

This thesis is accepted on behalf of the faculty

of the institute by the following committee:

Philip R. Kyle

Advisor

Nelia W. Dunbar

Andrew Campbell

3 December 1998

Date